The Astrophysical Journal, 733:10 (20pp), 2011 May 20 doi:10.1088/0004-637X/733/1/10

ON MACHINE-LEARNED CLASSIFICATION OF VARIABLE STARS WITH SPARSE AND NOISY TIME-SERIES DATA

Joseph W. Richards[1,2], Dan L. Starr[1], Nathaniel R. Butler[1], Joshua S. Bloom[1], John M. Brewer[3], Arien Crellin-Quick[1], Justin Higgins[1], Rachel Kennedy[1], and Maxime Rischard[1]
[1] Astronomy Department, University of California, Berkeley, CA 94720-7450, USA; jwrichar@stat.berkeley.edu
[2] Statistics Department, University of California, Berkeley, CA 94720-7450, USA
[3] Astronomy Department, Yale University, New Haven, CT 06520-8101, USA

Received 2011 January 10; accepted 2011 March 13; published 2011 April 27

ABSTRACT

With the coming data deluge from synoptic surveys, there is a need for frameworks that can quickly and automatically produce calibrated classification probabilities for newly observed variables based on small numbers of time-series measurements. In this paper, we introduce a methodology for variable-star classification, drawing from modern machine-learning techniques. We describe how to homogenize the information gleaned from light curves by selection and computation of real-numbered metrics (features), detail methods to robustly estimate periodic features, introduce tree-ensemble methods for accurate variable-star classification, and show how to rigorously evaluate a classifier using cross validation. On a 25-class data set of 1542 well-studied variable stars, we achieve a 22.8% error rate using the random forest (RF) classifier; this represents a 24% improvement over the best previous classifier on these data. This methodology is effective for identifying samples of specific science classes: for pulsational variables used in Milky Way tomography we obtain a discovery efficiency of 98.2% and for eclipsing systems we find an efficiency of 99.1%, both at 95% purity. The RF classifier is superior to other methods in terms of accuracy, speed, and relative immunity to irrelevant features; the RF can also be used to estimate the importance of each feature in classification. Additionally, we present the first astronomical use of hierarchical classification methods to incorporate a known class taxonomy in the classifier, which reduces the catastrophic error rate from 8% to 7.8%. Excluding low-amplitude sources, the overall error rate improves to 14%, with a catastrophic error rate of 3.5%.

Key words: methods: data analysis – methods: statistical – stars: variables: general – techniques: photometric

1. INTRODUCTION

Variable-star science (e.g., Eyer & Mowlavi 2008) remains at the core of many of the central pursuits in astrophysics: *pulsational* sources probe stellar structure and stellar evolution theory, *eruptive* and *episodic* systems inform our understanding of accretion, stellar birth, and mass loss, and *eclipsing* systems constrain mass transfer, binary evolution, exoplanet demographics, and the mass–radius–temperature relation of stars. Some eclipsing systems and many of the most common pulsational systems (e.g., RR Lyrae, Cepheids, and Mira variables) are the fundamental means to determine precise distances to clusters, to relic streams of disrupted satellites around the Milky Way, and to the local group of galaxies. They anchor the measurement of the size scale of the universe. See Walkowicz et al. (2009) for a recent review.

The promise of modern synoptic surveys (Ivezić et al. 2007), such as the Large Synoptic Survey Telescope (LSST), is the promise of discovery of many new instances of variable stars (Sesar et al. 2007), some to be later studied individually with greater photometric and spectroscopic scrutiny[4] and some to be used as ensemble probes to larger volumes. New classes (with variability reflecting physics not previously seen) and rare instances of existing classes of variables are almost certainly on the horizon (e.g., Covey et al. 2007).

Classification of variable stars—the identification of a certain variable with a previously identified group (“class”) of sources presumably of the same physical origin—presents several challenges. First, time-series data alone (i.e., without spectroscopy) provide an incomplete picture of a given source: this picture is even less clear the more poorly sampled the light curve is both in time and in precision. Second, on conceptual grounds, the observation of variability does not directly reveal the underlying physical mechanisms responsible for the variability. What the totality of the characteristics *are* that define the nature of the variability may in principle be known at the statistical level. But *why* that variability is manifest relies on an imperfect mapping of an inherently incomplete physical model to the data. (For example, the periodic dimming of a light curve may be captured with a small number of observable parameters but the inference that source is an eclipsing one requires a theoretical framework.) This intermingling of observation and theory has given rise to a taxonomy of variable stars (for instance, defined in the GCVS[5]) that is based on an admixture of phenomenology and physics. Last, on logistical grounds, the data volume of time-series surveys may be too large for human-intensive analysis, follow-up, and classification (which benefits from domain-specific knowledge and insight).

While the data deluge problem suggests an obvious role for computers in classification,[6] the other challenges also naturally lend themselves to algorithmic and computational solutions. Individual light curves can be automatically analyzed with a variety of statistical tools and the outcome of those analyses can be handled with machine-learning algorithms that work with existing taxonomies (however, fuzzy the boundary between classes) to produce statistical statements about the source classification. Ultimately, with a finite amount of time-series

[4] High-precision photometry missions (*Kepler*, *MOST*, *CoRoT*, etc.) are already challenging the theoretical understanding of the origin of variability and the connection of some specific sources to established classes of variables.

[5] General Catalog of Variable Stars: http://www.sai.msu.su/groups/cluster/gcvs/gcvs/.

[6] Not discussed herein are the challenges associated with the *discovery* of variability. See Shin et al. (2009) for a review.

data we wish to have well-calibrated probabilistic statements about the physical origin and phenomenological class of that source.

While straightforward, in principle, providing a machine-learned classifier that is accurate, fast, and well calibrated is an extraordinarily difficult task on many fronts (see the discussion in Eyer et al. 2008). There may be only a few instances of light curves in a given class ("labeled data") making training and validation difficult. Even with many labeled instances, in the face of noisy, sometimes spurious, and sparsely sampled data, there is a limit to the statistical inferences that can be gleaned from a single light curve. Some metrics (called "features") on the light curve may be very sensitive to the signal-to-noise ratio (S/N) of the data and others, particularly frequency-domain features, may be sensitive to the precise cadences of the survey (Section 4.9). For computationally intensive feature generation (e.g., period searches), fast algorithms may be preferred over slower but more robust algorithms.

Machine learning in variable-star classification has been applied to several large time-series data sets (Belokurov et al. 2003, 2004; Woźniak et al. 2004; Willemsen & Eyer 2007; Debosscher et al. 2007; Mahabal et al. 2008; Sarro et al. 2009; Blomme et al. 2010). A common thread for most previous work is application of a certain machine-learning framework to a single survey. And, most often, the classification is used to distinguish/identify a small set of classes of variables (e.g., Miras and other red giant variability). Debosscher et al. (2007) was the first work to tackle the many-class (>20) problem with multiple survey streams. Debosscher et al. (2007) also explored several classification frameworks and quantitatively compared the results.

The purpose of this work is to build a many-class classification framework by exploring in detail each aspect of the classification of variable stars: proper feature creation and selection in the presence of noise and spurious data (Section 2), fast and accurate classification (Section 3), and improving classification by making use of the taxonomy. We present a formalism for evaluating the results of the classification in the context of expected statistical risk for classifying new data. We use data analyzed by Debosscher et al. to allow us to make direct comparison with those results (Section 4). Overall, we find a 24% improvement in the misclassification rate with the same data. The present work only makes use of metrics derivable from time-domain observations in a single bandpass; color information and context (i.e., the location of the variable in the Galaxy and with respect to other catalog sources) are not used. In future work, we will explore how machine-learned classifiers can be applied across surveys (with different characteristics) and how context and time-domain features can be used in tandem to improve overall classification.

2. HOMOGENIZING LIGHT CURVES: FEATURE GENERATION

Classification fundamentally relies upon the ability to recognize and quantify the differences between light curves. To build a (supervised) machine-learning classifier, many *instances* of light curves are required for each class of interest. These labeled instances are used in the *training* and *testing* process (Section 3). Since the data are not, in general, sampled at regular intervals nor are all instances of a certain class observed with the same number of epochs and S/N, identifying the differences directly from the time-series data is challenging both conceptually and computationally (cf. Eads et al. 2004). Instead, we homogenize the data by transforming each light curve into a set of real-number line features using statistical and model-specific fitting procedures. For variable stars, features fall into two broad categories: those that related to the period of the source (and harmonics) and those that are not. Which features to use (and not use) is an important question that we will address herein. We also address the effects of (implicit) correlation of certain features in affecting the classification model.

Appendix A provides an account of the non-periodic features used in this present work; many of these are simple statistics on the distribution of the fluxes (e.g., median absolute deviation and min–max amplitude) and some are domain specific (such as a feature that captures how much a source varies like the damped random walk seen in quasars; Butler & Bloom 2011). Since the period and periodic signatures of a variable are such crucial quantitative measurements, yet tend to be difficult to infer from simple prescriptions, we review the algorithms we employ to compute these features.

2.1. *Robust Estimation of Periodic Features*

2.1.1. *A Fast Period Search Including Measurement Uncertainty*

We model the photometric magnitudes of variable stars versus time t as a superposition of sines and cosines, starting from the most basic form

$$y_i(t|f_i) = a_i \sin(2\pi f_i t) + b_i \cos(2\pi f_i t) + b_{i,\circ}, \qquad (1)$$

where a and b are normalization constants for the sinusoids of frequency f_i, and $b_{i,\circ}$ is the magnitude offset. For each variable star, we record at each epoch, t_k, a photometric magnitude, d_k, and its uncertainty, σ_k. To search for periodic variations in these data, we fit Equation (1) by minimizing the sum of squares

$$\chi^2 = \sum_k [d_k - y_i(t_k)]^2/\sigma_k^2, \qquad (2)$$

where σ_k is the measurement uncertainty in data point d_k. As discussed in Zechmeister & Kürster (2009), this least-squares fitting of sinusoids with a floating mean and over a range of test frequencies is closely similar to an evaluation of the well-known Lomb–Scargle (Lomb 1976; Barning 1963; Scargle 1982) periodogram. Allowing the mean to float leads to more robust period estimates in the cases where the periodic phase is not uniformly sampled; in these cases, the model light curve has a non-zero mean. (This is particularly important for searching for periods on timescales similar to the data span $T_{\rm tot}$.) If we define

$$\chi^2_\circ = \sum_k [d_k - \mu]^2/\sigma_k^2 \qquad (3)$$

with the weighted mean $\mu = \sum_k [d_k/\sigma_k^2]/\sum_k 1/\sigma_k^2$, then our generalized Lomb–Scargle periodogram P_f is

$$P_f(f) = \frac{(N-1)}{2}\frac{\chi^2_\circ - \chi^2_m(f)}{\chi^2_\circ}, \qquad (4)$$

where $\chi^2_m(f)$ is χ^2 minimized with respect to a, b, and $b_\circ$. For the NULL hypothesis of no periodic variation and a white Gaussian noise spectrum, we expect P_f to be F-distributed with two numerator and $N-1$ denominator degrees of freedom. A similar periodogram statistic and NULL distribution is derived in Gregory (2005) by marginalizing over an unknown scale error in the estimation of the uncertainties. In the limit of many

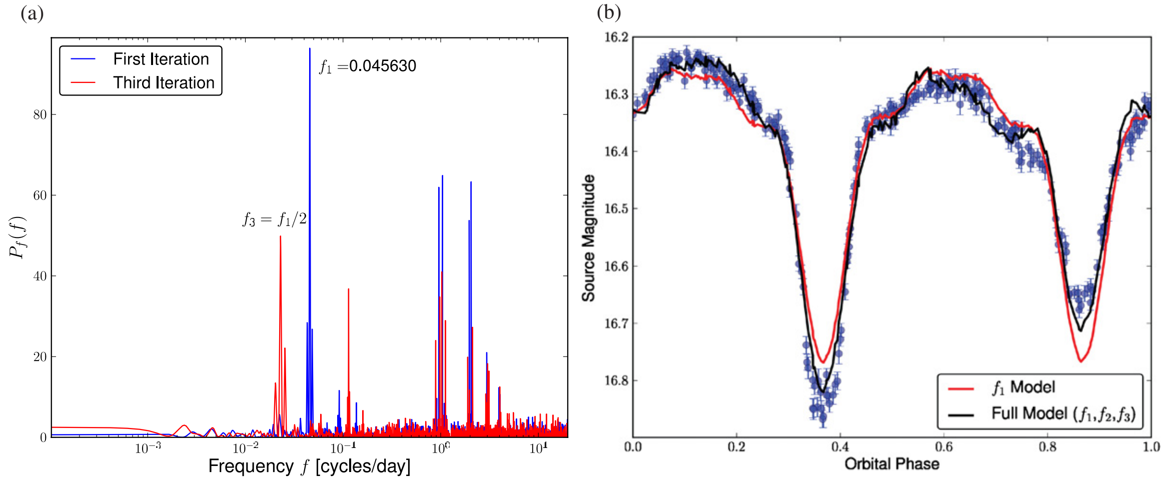

Figure 1. (a) Generalized Lomb–Scargle periodogram $P_f(f)$ for an eclipsing source in the sample. Plotted in blue is the first iteration to find peak frequency f_1, which is twice the orbital frequency f_3 (third iteration plotted in red). In this case, the second iteration yielded $f_2 = 3f_3$. For eclipsing sources, our $P_f(f)$ analysis which utilizes a sine and cosine fit without harmonics, tends to place the orbital period in either f_2 or f_3. (b) The light curve folded at the orbital period f_3. Overplotted is the best-fit model considering only f_1 (plus three harmonics; in red), which fails to account for the difference in primary and secondary eclipse depths. Addition of the second and third frequency component models (black curve) account for the full light-curve structure well.

data, the NULL distribution takes the well-known exponential form (e.g., Zechmeister & Kürster 2009). For all $\sigma_i = 1$, Equation (4) becomes the standard Lomb–Scargle periodogram. In addition to the benefits of allowing a floating mean, the generalized Lomb–Scargle periodogram (4) has two principal advantages over the standard formula: (1) uncertainties on the measurements are included and (2) scale errors in the determination of these uncertainties have no influence on the periodogram because $P(f)$ is a ratio of two sums of squares (cf. Gregory 2005).

We undertake the search for periodicity in each source by evaluating Equation (4) on a linear test grid in frequency from a minimum value of $1/T_{\rm tot}$ to a maximum value of 20 cycles per day, in steps of $\delta f = 0.1/T_{\rm tot}$. This follows closely the prescription in Debosscher et al. (2007), with the important exception that we search for periods up to 20 cycles per day in all sources, whereas Debosscher et al. (2007) search up to a “pseudo” Nyquist frequency ($f_N = 0.5\langle 1/\Delta T\rangle$, where ΔT is the difference in time between observations and $\langle\cdot\rangle$ is an average) for most sources but allow the maximum frequency value to increase for certain source classes. To avoid favoring spurious high-frequency peaks in the periodogram, we subtract a mild penalty of $\log f/f_N$ above f_N from $P_f(f)$ above $f = f_N$. Significance of the highest peak is evaluated from $P_f(f)$. We apply an approximate correction for the number of search trials using the prescription of Horne & Baliunas (1986), although we note that numerical simulations suggest that these significance estimates underestimate the number of true trials and are uniformly high by 1σ–2σ.

Standard “fast” implementations of the Lomb–Scargle periodogram (e.g., Press et al. 2001), which scale with the number of frequency bins N_f as $N_f \log N_f$, are not particularly fast for our purposes. This is because we wish to sample relatively few data ($N \sim 100$) on a very dense, logarithmic frequency grid $N_f \sim 10^6$. It is more fruitful to pursue algorithms which scale more strongly with N than N_f. We find that standard implementations, which scale as $N \cdot N_f$, are sped up by a factor of ~ 10, substantially outperforming $N_f \log(N_f)$ implementations, by simply taking care to efficiently calculate the sines and cosines that are necessary to tabulate Equation (4). Instead of calculating all the sines and cosines at a given time point at each of the N_f frequency bins, we calculate sine and cosine only once at $f = \delta f$ and then use trigonometric identities (i.e., successive rotations by an angle $2\pi\,\delta f\,t_i$) to determine the sines and cosines at higher frequencies.

2.1.2. *Fitting Multiple Periods*

Following Debosscher et al. (2007), we fit each light curve with a linear term plus a harmonic sum of sinusoids:

$$y(t) = ct + \sum_{i=1}^{3}\sum_{j=1}^{4} y_i(t|jf_i), \tag{5}$$

where each of the three test frequencies f_i is allowed to have four harmonics at frequencies $f_{i,j} = jf_i$. The three test frequencies f_i are found iteratively, by successfully finding and removing periodic signal producing a peak in $P_f(f)$. Given a peak in $P_f(f)$, we seek to whiten the data with respect to that frequency by fitting away a model containing that frequency as well as components with frequencies two, three, and four times that fundamental frequency. We then subtract this model from the data, update $\chi^2_\circ$, and recalculate $P_f(f)$ to find an additional periodic component. The procedure is repeated three times, to extract three frequencies as well as the statistics pertaining to the harmonic amplitudes, phases, and significance of each component. In Figure 1 we show the result of applying this iterative fitting procedure to the light curve of an eclipsing variable star.

In reporting the values from the fit of Equation (5), we ignore the constant offsets $b_{i,\circ}$. We translate the sinusoid coefficients into an amplitude and a phase

$$A_{i,j} = \sqrt{a_{i,j}^2 + b_{i,j}^2} \tag{6}$$

$$\mathrm{PH}_{i,j} = \tan^{-1}(b_{i,j}, a_{i,j}). \tag{7}$$

Here, $A_{i,j}$ ($\mathrm{PH}_{i,j}$) is the amplitude (phase) of the jth harmonic of the ith frequency component. Following Debosscher et al.

(2007), we correct the phases $\mathrm{PH}_{i,j}$ to relative phases with respect to the phase of the first component $\mathrm{PH}'_{i,j} = \mathrm{PH}_{i,j} - \mathrm{PH}_{00}$. This is to preserve comparative utility in the phases for multiple sources by dropping a non-informative phase offset for each source. All phases are then remapped to the interval $| -\pi, +\pi |$.

A list and summary of all of the period features used in our analysis is found in Table 4 in Appendix A.

2.2. Non-periodic Light Curve Features

In seeking to classify variable-star light curves, it may not always be possible to characterize flux variation purely by detecting and characterizing periodicity. We find that simple summary statistics of the flux measurements (e.g., standard deviation, skewness, etc.)—determined without sorting the data in time or period phase—give a great deal of predictive power. For instance, skewness is very effective for separating eclipsing from non-eclipsing sources. We define (in Appendix A) 20 non-periodic features and explore in Section 4 their utility for source classification. A summary of all of the non-period features used in our analysis is found in Table 5 in Appendix A.

When only a small number of epochs ($\lesssim$12) are sampled, we find that period detection becomes unreliable: we can only rely on crude summary statistics and contextual information to characterize these sources. In addition, some source classes yield non-period or multiply periodic light curves, whereby the non-periodic features are expected in these cases to carry useful additional information not already contained in the periodic features. As an example, we apply metrics used in the time-domain study of quasars (Butler & Bloom 2011) to aid in disentangling the light curves of some complexly varying, long-period variables (e.g., semiregular pulsating variables). These quasar metrics are derived from a simple model of time-correlated variations not captured by our other features.

3. CLASSIFICATION FRAMEWORKS FOR VARIABLE STARS

The features extracted from a light curve give a characterization of the observed astronomical source. We need a rigorous way of turning this information into a probabilistic statement about the science class of that source. This is the goal of (supervised) classification: given a set of sources whose science class is known, learn a model that describes each source's class probabilities as a function of its features. This model is then used to automatically predict the class probabilities, and the most likely science class, of each new source.

Several authors have used machine-learning methods to classify variable stars using their light curves: Brett et al. (2004) use Kohonen self-organizing maps, Eyer & Blake (2005) use the Bayesian mixture-model classifier `Autoclass` (Cheeseman & Stutz 1996, p. 180), and Debosscher et al. (2007) experiment with several methods, including Gaussian mixture models, Bayesian networks, Bayesian averaging of artificial neural networks, and support vector machines (SVMs). All of these methods have certainly enjoyed widespread use in the literature and are a reasonable first set of tools to use in classifying variable stars. Our major contribution in this section is to introduce tree-based classification methods—including classification and regression trees (CART), random forests (RFs), and boosted trees—for the classification of variable stars. Tree-based classifiers are powerful because they are able to capture complicated interaction structure within the feature space, are robust to outliers, naturally handle multi-class problems, are resilient to irrelevant features, easily cope with missing feature values, and are computationally efficient and scalable for large problems. Furthermore, they are simple to interpret and explain and generally yield accurate results. In Section 4, we show the superior performance of tree-based methods over the methods used in Debosscher et al. (2007) for classifying variable stars.

Below, we describe several tree-based classification approaches from the statistics and machine-learning literature, showing how to train each classifier and how to predict science-class probabilities for each observed source. We also introduce a suite of pairwise voting classifiers, where the multi-class problem of variable-star classification is simplified into a set of two-class problems and the results are aggregated to estimate class probabilities. Additionally, we outline a procedure for incorporating the known variable-star class taxonomy into our classifier. Finally, we describe a rigorous risk-based framework to choose the optimal tuning parameter(s) for each classifier and show how to objectively assess the expected performance of each classifier through cross validation.

3.1. Tree-based Classifiers

Decision tree learning has been a popular method for classification and regression in statistics and machine learning for more than 20 years (Breiman et al. 1984 popularized this approach). Recently, the astronomical community has begun to use tree-based techniques, for several problems. For example, tree-based classifiers have been used by Suchkov et al. (2005) for Sloan Digital Sky Survey (SDSS) object classification, by Ball et al. (2006) and O'Keefe et al. (2009) for star–galaxy separation, by Bailey et al. (2007) to identify supernova candidates, and by several groups for supernova classification in the recent DES Supernova Photometric Classification Challenge (Kessler et al. 2010).

Tree-based learning algorithms use recursive binary partitioning to split the feature space, $\mathcal{X}$, into disjoint regions, $R_1, R_2, \ldots, R_M$. Within each region, the response is modeled as a constant. Every split is performed with respect to one feature, producing a partitioning of $\mathcal{X}$ into a set of disjoint rectangles (nodes in the tree). At each step, the algorithm selects both the feature and split point that produces the smallest impurity in the two resultant nodes. The splitting process is repeated, recursively, on all regions to build a tree with multiple levels.

In this section, we give an overview of three tree-based methods for classification: classification trees, RF, and boosting. We focus on the basic concepts and a few particular challenges in using these classifiers for variable-star classification. For further details about these methods, we refer the interested reader to Hastie et al. (2009).

3.1.1. Classification Trees

To build a classification tree, begin with a training set of (feature, class) pairs $(\mathbf{X}_1, Y_1), \ldots, (\mathbf{X}_n, Y_n)$, where Y_i can take any value in $\{1, \ldots, C\}$. At node m of the tree, which represents a region R_m of the feature space $\mathcal{X}$, the probability that a source with features in R_m belongs to class c is estimated by

$$\widehat{p}_{mc} = \frac{1}{N_m} \sum_{\mathbf{X}_i \in R_m} I(Y_i = c), \quad (8)$$

which is the proportion of the N_m training set objects in node m whose science class is c, where $I(Y_i = c)$ is the indicator function defined to be 1 if $Y_i = c$ and 0 else. In the tree-building process, each subsequent split is chosen among all possible features and split points to minimize a measure of the resultant node impurity, such as the Gini index ($\sum_{c\neq c'}^{C} \widehat{p}_{mc}\widehat{p}_{mc'}$) or entropy ($-\sum_{c=1}^{C} \widehat{p}_{mc} \log_2 \widehat{p}_{mc}$). The Gini index is the measure of choice for CART (Breiman et al. 1984), while entropy is used by the popular algorithm C4.5 (Quinlan 1996). This splitting process is repeated recursively until some pre-defined stopping criterion (such as minimum number of observations in a terminal node, or relative improvement in the objective function) is reached.

Once we have trained a classification tree on the examples $(\mathbf{X}_1, Y_1), ..., (\mathbf{X}_n, Y_n)$, it is straightforward to ingest features from a new instance, $\mathbf{X}_{\text{new}}$, and predict its science class. Specifically, we first identify which tree partition $\mathbf{X}_{\text{new}}$ resides in and then assign it a class based on that node's estimated probabilities from Equation (8). For example, if $\mathbf{X}_{\text{new}} \in R_m$, then the classification-tree probability that the source is in class c is

$$\widehat{p}_c(\mathbf{X}_{\text{new}}) = \widehat{p}_{mc}, \tag{9}$$

where $\widehat{p}_{mc}$ is defined in Equation (8). Using Equation (9), the predicted science class is $\widehat{p}(\mathbf{X}_{\text{new}}) = \arg\max_c \widehat{p}_c(\mathbf{X}_{\text{new}})$. Note that we are free to describe the classification output for each new source either as a vector of class probabilities or as its predicted science class.

There remains the question of how large of a tree should be grown. A very large tree will fit the training data well, but will not generalize well to new data. A very small tree will likely not be large enough to capture the complexity of the data-generating process. The appropriate size of a tree ultimately depends on the complexity of model necessary for the particular application at hand and hence should be determined by the data. The standard approach to this problem is to build a large tree, T, with M terminal nodes and then to *prune* this tree to find the subtree T^* of T that minimizes a cross-validation estimate of its statistical risk (see Section 3.5).

3.1.2. Random Forest

Classification trees are simple, yet powerful, non-parametric classifiers. They work well even when the true model relating the feature space to the class labeling is complicated, and generally yield estimates with very small bias. However, tree models tend to have high variance. Small changes in the training set features can produce very different estimated tree structure. This is a by-product of the hierarchical nature of the tree model: small differences in the top few nodes of a tree can produce wildly different structure as those perturbations are propagated down the tree. To reduce the variance of tree estimates, *bagging* (bootstrap aggregation; Breiman 1996) was proposed to average the predictions of B trees fitted to bootstrapped samples of the training data. *Random forest* (Breiman 2001) is an improvement to bagging that attempts to de-correlate the B trees by selecting a random subset of m_{try} of the input features as candidates for splitting at each node during the tree-building process. The net result is that the final, averaged RF model has lower variance than the bagging model, while maintaining a small bias (see Hastie et al. 2009, Chapter 15 for a discussion).

To obtain an RF classification model, we grow B de-correlated classification trees. For a new variable star, the class probabilities are estimated as the proportion of the B trees that predict each class. As in classification trees, we are free to describe each source as a vector of class probabilities or a best-guess class. This prescription generally works well because by averaging the predictions over many bootstrapped trees, the estimated probabilities are more robust to chance variations in the original training set and are almost always more accurate than the output of a single tree. Another advantage to RF is the relative robustness of the estimates to choices of the tuning parameters (B, m_{try}, and the size of each tree) compared to other non-parametric classification techniques. In practice, we use the parameter values that give minimal cross-validation risk.

3.1.3. Boosted Trees

Boosting is a method of aggregating simple rules to create a predictive model whose performance is "boosted" over that of any of its ensemble members (Freund & Schapire 1996). In classification boosting, a sequence of simple classifiers (referred to as weak learners) is applied, whereby in each iteration the training observations are re-weighted so that those sources which are repeatedly misclassified are given greater influence in the subsequent classifiers. Therefore, as the iterations proceed, the classifier pays more attention to data points that are difficult to classify, yielding improved overall performance over that of each weak learner. The predicted class probabilities are obtained from a weighted estimate of the individual classifiers, with weights proportional to the accuracy of each classifier.

Classification trees are natural base learners in a boosting algorithm because of their simplicity, interpretability, and ability to deal with data containing outliers and missing values. Moreover, there are efficient algorithms that can quickly estimate boosted trees using gradient boosting (Friedman 2001). It is usually sufficient to use single-split trees (so-called decision stumps) as base learners, though in situations with more complicated interactions, bigger trees are necessary. We use the training data to adjust the pruning depth through cross validation.

3.2. Measuring Feature Importance

An additional advantage to tree-based classifiers is that, because the trees are constructed by splitting one feature at a time, they allow us to estimate the importance of each feature in the model. A feature's importance can be deduced by, for instance, counting how often that feature is split or looking at the resultant decrease in node impurity for splits on that feature. Additionally, RF provides a measure of the predictive strength of each feature, referred to as the *variable importance*, which tells us roughly what the decrease in overall classification accuracy would be if a feature were replaced by a random permutation of its values. RF has a rapid procedure for estimating variable importance via its *out-of-bag* samples for each tree, those data that were not included in the bootstrapped sample.

Analyzing the feature importance is a critical step in building an accurate classification model. By determining which features are important for distinguishing certain classes, we gain valuable insight into the physical differences between particular science classes. Moreover, we can visualize which types of features are more predictive than others, which can inform the use of novel features or the elimination of useless features in a second-generation classifier.

3.3. Pairwise Classifiers

A common approach for multi-class classification is to reduce the C-class problem into a set of $C(C-1)/2$ pairwise comparisons. This is a viable approach because two-class problems are usually easier to solve since the class boundaries tend to be relatively simple. Moreover, some classification methods,

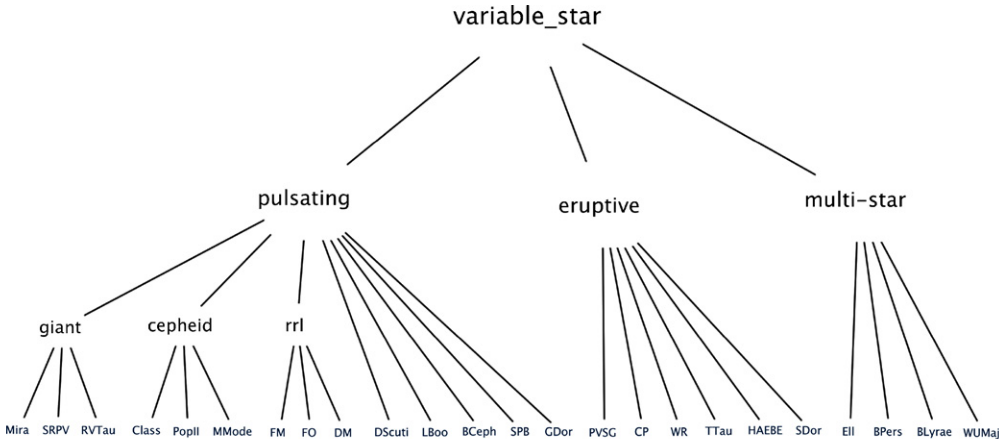

Figure 2. Variable-star classification hierarchy for the data used in Section 4. This structure is a crucial element of the two hierarchical classifiers used in this study, HSC and HMC. The hierarchy is constructed based on knowledge of the physical processes that govern each type of object. At the top level, the sources split into three major categories: pulsating, eruptive, and multi-star systems.

such as SVMs (Vapnik 2000), are designed to work only on two-class problems. In pairwise classification, classifiers for all $C(C-1)/2$ two-class problems are constructed. The challenge, then, is to map the output from the set of pairwise classifiers for each source (pairwise probabilities or class indicators) to a vector of C-class probabilities that accurately reflects the science class of that source. This problem is referred to as pairwise coupling.

The simplest method of pairwise coupling is voting (Knerr et al. 1990; Friedman 1996), where the class of each object is determined as the winner in a pairwise head-to-head vote. Pairwise voting is suboptimal because it ignores the pairwise class probabilities and tends to estimate inaccurate C-class probabilities. In situations where pairwise class probability estimates are available, voting is outperformed by other methods such as that of Hastie & Tibshirani (1998), which attempts to minimize the Kullback–Leibler distance between the observed pairwise probabilities and those induced by the C-class probabilities, and the approaches of Wu et al. (2004), which minimize a related discrepancy measure that reduces to solving a linear system of equations. In this paper, we explore the use of both tree-based classifiers and SVMs in pairwise classifiers. To obtain C-class probabilities, we employ the second pairwise coupling method introduced by Wu et al. (2004). We refer the interested reader to that paper for a more detailed description of the method and a review of similar techniques in the literature.

3.4. Hierarchical Classification

In variable-star classification, we have at our disposal a well-established hierarchical taxonomy of classes based on the physics and phenomenology of these stars and stellar systems. For instance, at the top level of our taxonomy, we can split the science classes into three main categories: pulsating, eruptive, and multi-star systems. From there, we can continue to divide the subclasses until we are left with exactly one of the original 25 science classes in each node (see Figure 2). For classification purposes, the meaning of the hierarchy is clear: mistakes at the highest levels of the hierarchy are more costly than mistakes made at deeper levels because the top levels of the hierarchy divide physical classes that are considerably different, whereas deeper levels divide subclasses that are quite similar.

Incorporating a known class hierarchy, such as that of Figure 2, into a classification engine is a research field that has received much recent attention in the machine-learning literature (see Silla & Freitas 2011 for a survey of these methods). By considering the class hierarchy, these classifiers generally outperform their "flat classifier" counterparts because they impose higher penalties on the more egregious classification errors. In this paper, we consider two types of hierarchical classification approaches: hierarchical single-label classification (HSC; Cesa-Bianchi et al. 2006) and hierarchical multi-label classification (HMC; Blockeel et al. 2006, p. 18). We implement both HSC and HMC using RFs of decision trees. Below, we provide a synopsis of HSC and HMC. For more details about these methods, see Vens et al. (2008).

In HSC, a separate classifier is trained at each non-terminal node in the class hierarchy, whereby the probabilities of each classifier are combined using conditional probability rules to obtain each of the class probabilities. This has a similar flavor to the pairwise classifier approach of Section 3.3, but by adhering to the class hierarchy it needs only to build a small set of classifiers and can generate class probabilities in a straightforward, coherent manner. Moreover, different classifiers and/or sets of features can be used at each node in HSC, allowing for the use of more general classifiers at the top of the hierarchy and specialized domain-specific classifiers deeper in the hierarchy. A recent paper of Blomme et al. (2010) applied a method similar to HSC, using Gaussian mixture classifiers, to classify variable stars observed by the *Kepler* satellite. A second hierarchical classification approach is HMC, which builds a single classifier in which errors on the higher levels of the class hierarchy are penalized more heavily than errors deeper down the hierarchy. In the version of HMC that we use, the weight given to a classification error at depth d in the class hierarchy is w_0^d, where $w_0 \in (0, 1)$ is a tuning parameter. This forces the algorithm to pay more attention to the top level, minimizing the instances of catastrophic error (defined in Section 4.3).

3.5. Classifier Assessment through Cross Validation

We have introduced a few methods that, given a sample of training data, estimate a classification model, $\widehat{p}$, to predict the science class of each new source. In this section, we introduce statistically rigorous methodology for assessing each classifier and choosing the best classifier among a set of alternatives. Since our ultimate goal is to accurately classify newly collected data, we will use the classifier that gives the best expected performance on new data. We achieve this by defining a classifier's *statistical risk* (i.e., prediction error) and computing an unbiased estimate of that risk via *cross validation*. We will ultimately use the model that obtains the smallest risk estimate.

Given a new source of class Y, having features $\mathbf{X}$, we define a loss function, $L(Y, \widehat{p}(\mathbf{X}))$, describing the penalty incurred by the application of our classifier, $\widehat{p}$, on that source. The loss function encompasses our notion of how much the classifier $\widehat{p}$ has erred in predicting the source's class from its features $\mathbf{X}$. The expected value of L, $E[L(Y, \widehat{p}(\mathbf{X}))]$, is the statistical risk, $R(\widehat{p})$, of the classifier. The expected value, $E[\cdot]$, averages over all possible realizations of $(\mathbf{X}, Y)$ to tell us how much loss we can expect to incur for the predicted classification of each new source (under the assumption that new data are drawn from the same distribution as the training data). A key aspect to this approach is that it guards against overfitting to the training data: if a model is overly complex, it will only add extra variability in classification without decreasing the bias of the classifier, leading to an increase in the risk (this is the bias-variance trade-off; see Wasserman 2006).

Conveniently, within this framework each scientist is free to tailor the loss function to meet their own scientific goals. For instance, an astronomer interested in finding Mira variables could define a loss function that incurs higher values for misclassified Miras. In this work, we use the vanilla 0–1 loss that is defined to be 0 if $Y = \widehat{p}(\mathbf{X})$ and 1 if misclassified (here, $\widehat{p}(\mathbf{X})$ is the estimated class of the source; alternatively, we could define a loss function over the set of estimated class probabilities, $\{\widehat{p}_1(\mathbf{X}), ..., \widehat{p}_C(\mathbf{X})\}$). Under 0–1 loss, the statistical risk of a classifier is its expected overall misclassification rate, which we aim to minimize.

There remains the problem of how to estimate the statistical risk, $R(\widehat{p})$ of a classifier $\widehat{p}$. If labeled data were plentiful, we could randomly split the sources into training and validation sets, estimating $\widehat{p}$ with the training set and computing a risk estimate $\widehat{R}(\widehat{p})$ with the validation set. Since our data are relatively small in number, we use k-fold cross validation to estimate R. In this procedure, we first split the data into K (relatively) equal-sized parts. For each subset $k = 1, ..., K$, the classifier is fitted on all of the data not in k and a risk estimate, $\widehat{R}_{(-k)}(\widehat{p})$, is computed on the data in set k. The cross-validation risk estimate is defined as $\widehat{R}_{\rm CV}(\widehat{p}) = \frac{1}{K}\sum_{k=1}^{K}\widehat{R}_{(-k)}(\widehat{p})$. As shown in Burman (1989), for $K \gtrsim 4$, $\widehat{R}_{\rm CV}(\widehat{p})$ is an approximately unbiased estimate of $R(\widehat{p})$. In this paper, we use $K = 10$ fold cross validation.

In addition to selecting between different classification models, cross-validation risk estimates can be used to choose the appropriate tuning parameter(s) for each classifier. For instance, we use cross validation to choose the optimal pruning depth for classification trees, to pick the optimal number and depth of trees to build, and number of candidate splitting features to use at each split for RFs, and to select the optimal size of the base learner, number of trees, and learning rate for boosted decision trees. The optimal set of tuning parameters for each method is found via a grid search. For each of the methods considered, we find that $\widehat{R}_{\rm CV}$ is stable in the neighborhood of the optimal tuning parameters, signifying that the classifiers are relatively robust to the specific choice of tuning parameters and that a grid search over those parameters is sufficient to obtain near-optimal results.

Table 1
Data Set Characteristics by Survey

Survey	NLC[a]	%NLC$_{\rm deb}$[b]	NLC Used[c]	$\langle T_{\rm tot}\rangle$ (days)[d]	$\langle N_{\rm epochs}\rangle$
Hipparcos	1044	100.0	1019	1097	103
OGLE	523	99.2	523	1067	329

Notes.
[a] Total number of light curves available to us.
[b] Percentage of Debosscher et al. (2007) light curves available to us.
[c] Number of light curves after the removal of sources with ambiguous class and exclusion of small classes.
[d] Average time baseline.

4. CLASSIFIER PERFORMANCE ON OGLE+*HIPPARCOS* DATA SET

4.1. Description of Data

In this paper, we test our feature extraction and classification methods using a mixture of variable-star photometric data from the OGLE and *Hipparcos* surveys. Optical Gravitational Lensing Experiment (OGLE; Udalski et al. 1999) is a ground-based survey from Las Campanas Observatory covering fields in the Magellanic Clouds and Galactic bulge. *Hipparcos* Space Astrometry Mission (Perryman et al. 1997) was an ESA project designed to precisely measure the positions of more than one hundred thousand stars. The data selected for this paper are the OGLE and *Hipparcos* sources analyzed by Debosscher et al. (2007), totaling 90% of the variable stars studied in that paper. A summary of the properties, by survey, of the data used in our study, is in Table 1. The light-curve data and classifications used for each source can be obtained through our `dotastro.org` light-curve repository.[7]

This sample was designed by Debosscher et al. (2007) to provide a sizable set of stars within each science class, for a broad range of classes. Our sample contains stars from the 25 science classes analyzed in their paper. Via an extensive literature search, they obtained a set of confirmed stars of each variability class. In Table 2 we list, by science class, the proportion of stars in that data set that we have available for this paper. Since the idea of their study was to capture and quantify the typical variability of each science class, the light curves were pre-selected to be of good quality and to have an adequate temporal sampling for accurate characterization of each science class. For example, the multi-mode Cepheid and double-mode RR Lyrae stars, which have more complicated periodic variability, were sampled from OGLE because of its higher sampling rate.

In our sample, there are 25 objects that are labeled as two different science classes. Based on a literature search of these stars, we determine that 14 of them reasonably belong to just a single class (five S Doradus, two Herbig AE/BE, three Wolf–Rayet (W-R), two Delta Scuti, one Mira, and one Lambda Bootis). The other 11 doubly labeled stars, which are listed in Table 6, were of an ambiguous class or truly belonged to two different classes, and were removed from the sample. See Appendix B for a detailed analysis and references for the doubly labeled objects. Because the sample was originally constructed by Debosscher et al. (2007) to consist only of well-understood stars with confident class labeling, we are justified in excluding these sources.

[7] http://dotastro.org/lightcurves/project.php?Project_ID=123

Table 2
Data Set Characteristics by Science Class

Variable Star Class	Name$_{\rm deb}$[a]	NLC[b]	%NLC$_{\rm deb}$	Instrument	$\langle N_{\rm epochs}\rangle$	min(f_1)[c]	$\langle f_1\rangle$[c]	max(f_1)[c]
a. Mira	MIRA	144	100.0	*Hipparcos*	98	0.0020	0.09	11.2508
b. Semireg PV	SR	42	100.0	*Hipparcos*	99	0.0010	0.15	1.0462
c. RV Tauri	RVTAU	6	46.2	*Hipparcos*	104	0.0012	0.05	0.1711
d. Classical Cepheid	CLCEP	191	97.9	*Hipparcos*	108	0.0223	0.15	0.4954
e. Pop. II Cepheid	PTCEP	23	95.8	*Hipparcos*	107	0.0037	0.21	0.7648
f. Multi. Mode Cepheid	DMCEP	94	98.9	OGLE	181	0.5836	1.21	1.7756
g. RR Lyrae, FM	RRAB	124	96.1	*Hipparcos*	91	1.2149	1.95	9.6197
h. RR Lyrae, FO	RRC	25	86.2	*Hipparcos*	92	2.2289	3.15	4.3328
i. RR Lyrae, DM	RRD	57	100.0	OGLE	304	2.0397	2.61	2.8177
j. Delta Scuti	DSCUT	114	82.0	*Hipparcos*	129	0.0044	7.90	19.7417
k. Lambda Bootis	LBOO	13	100.0	*Hipparcos*	84	7.0864	12.36	19.8979
l. Beta Cephei	BCEP	39	67.2	*Hipparcos*	96	0.0014	4.94	10.8319
m. Slowly Puls. B	SPB	29	61.7	*Hipparcos*	101	0.1392	1.09	11.8302
n. Gamma Doradus	GDOR	28	80.0	*Hipparcos*	95	0.2239	2.24	9.7463
o. Pulsating Be	BE	45	78.9	*Hipparcos*	106	0.0011	2.12	14.0196
p. Per. Var. SG	PVSG	55	72.4	*Hipparcos*	102	0.0015	3.41	15.7919
q. Chem. Peculiar	CP	51	81.0	*Hipparcos*	105	0.0076	2.57	13.4831
r. Wolf-Rayet	W-R	41	65.1	*Hipparcos*	99	0.0011	6.56	19.2920
s. T Tauri	TTAU	14	82.4	*Hipparcos*	67	0.0013	1.85	11.2948
t. Herbig AE/BE	HAEBE	15	71.4	*Hipparcos*	83	0.0009	1.41	10.0520
u. S Doradus	LBV	7	33.3	*Hipparcos*	95	0.0008	0.20	0.5327
v. Ellipsoidal	ELL	13	81.2	*Hipparcos*	105	0.1070	1.37	3.5003
w. Beta Persei	EA	169	100.0	OGLE	375	0.0127	0.93	3.1006
x. Beta Lyrae	EB	145	98.6	OGLE	365	0.0175	0.71	4.5895
y. W Ursae Maj.	EW	58	98.3	OGLE	369	0.2232	2.44	8.3018

Notes.
[a] Class name in Debosscher et al. (2007).
[b] Total number of light curves used, after the removal of ambiguous sources.
[c] f_1 is the frequency of the first harmonic in day^{-1}, estimated by the methodology in Section 2.1. Note that f_1 is misestimated for a few of the sources.

4.2. Classwise Distribution of Light-curve Features

Using the methodology in Section 2, we estimate features for each variable star in the data set using their light curve. The feature-extraction routines take 0.8 s per light curve, giving us a 53-dimensional representation of each variable star. The computations are performed in `Python` and `C` using a non-parallelized, single thread on a 2.67 GHz Intel Xeon X5550 CPU running on a v2.6.18 linux kernel machine. We estimate that the periodic-feature routines account for 75% of the computing time and scale linearly with the number of epochs in the light curve. Note that these metrics do not take into account the CPU time needed to read the XML data files from disk and load the data into memory.

Plots of one-dimensional density estimates, by science class, of a selected set of features are in Figure 3. These classwise feature distributions allow us to quickly and easily identify the differences, in feature space, between individual variable-star science classes. Density plots are very useful for this visualization because they provide a complete feature-by-feature characterization of each class, showing any multi-modality, outliers, and skewness in the feature distributions. For instance, it is immediately obvious that several of the eruptive-type variable-star classes have an apparent bi-modal or relatively flat frequency distributions, likely attributed to their episodic nature. Conversely, the RR Lyrae frequency distributions are all narrow and peaked, showing that indeed these stars are well characterized by the frequency of their flux oscillations. The feature density plots also inform us of which feature(s) are important in separating different sets of classes. For example, the RR Lyrae, FO and RR Lyrae, DM stars have overlapping distributions for each of the features in Figure 3 except the feature QSO, where their distributions are far apart, meaning that QSO will be a useful classification feature in separating stars of those two classes.

4.3. Classifier Comparison

In this section, we compare the different classification methods introduced in Section 3. To fit each classifier, except HMC–RF, we use the statistical environment `R`.[8] To fit HMC–RF, we use the open-source decision tree and rule learning system `Clus`.[9] Each of the classifiers was tuned via a grid search over the relevant tuning parameters to minimize the cross-validation misclassification rates. To evaluate each classifier, we consider two separate metrics: the overall misclassification error rate and the catastrophic error rate. We define catastrophic errors to be any classification mistake in the top level of the variable-star hierarchy in Figure 2 (i.e., pulsating, eruptive, multi-star). The performance measures for each classifier, averaged over 10 cross-validation trials, are listed in Table 3. In terms of overall misclassification rate, the best classifier is an RF with $B = 1000$ trees, achieving a 22.8% average misclassification rate. In terms of catastrophic error rate, the HSC–RF classifier with $B = 1000$ trees achieves the lowest value, 7.8%. The processing time required to fit the ensemble methods is greater than the time needed to fit single-tree models. However, this should not be viewed as a limiting factor: once any of these models is fit, predictions for new data can be produced very rapidly. For example, for an RF classifier of 1000 trees, class probability estimates

[8] `R` is a freely available language and environment for statistical computing and graphics available at http://cran.r-project.org/.
[9] http://dtai.cs.kuleuven.be/clus/index.html

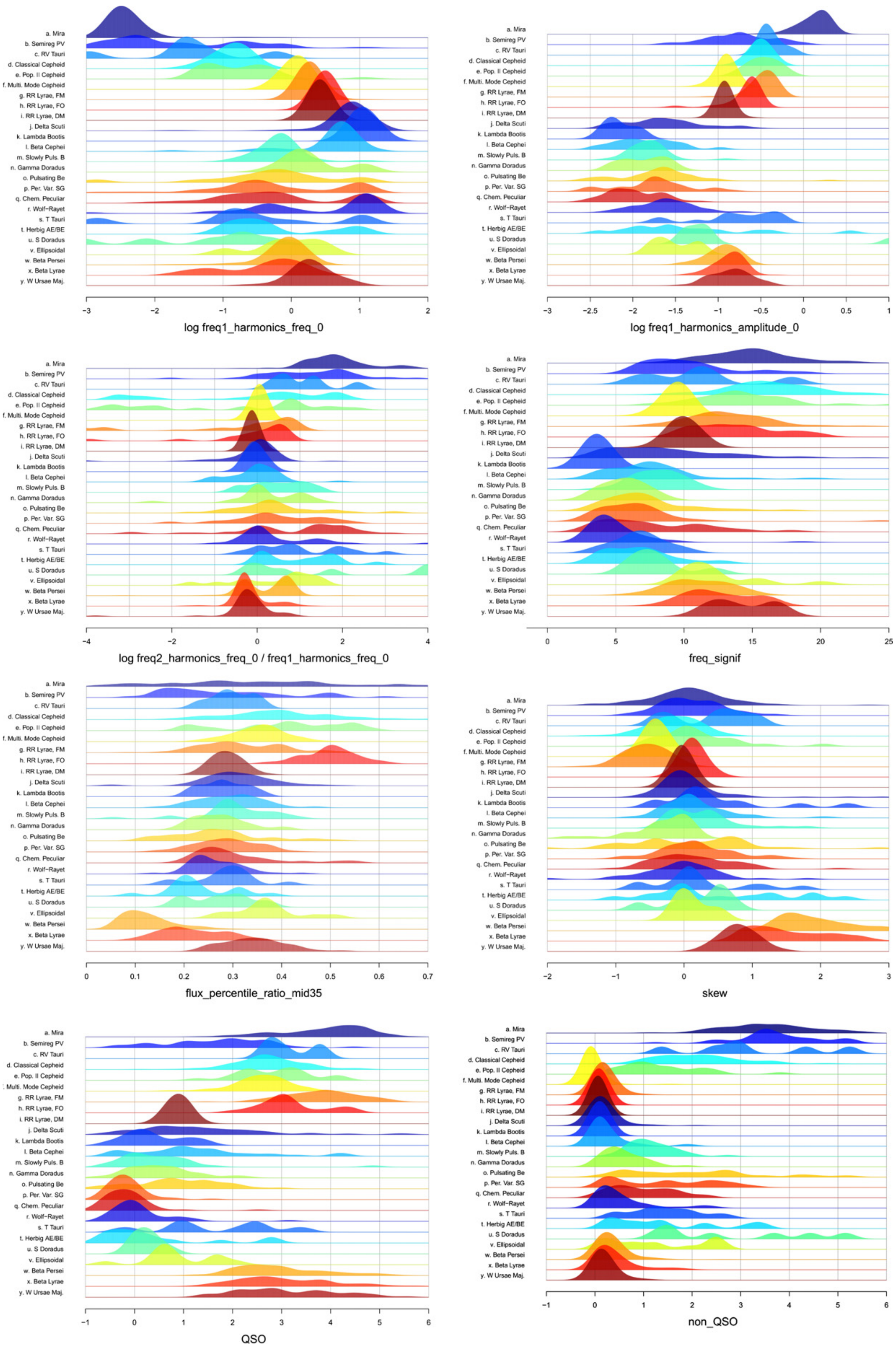

Figure 3. Histograms of several features by class. The features plotted are (a) the first frequency in cycles day^{-1}, (b) amplitude of the first frequency in mag, (c) the ratio of the second to the first frequencies, (d) statistical significance of the periodic model, (e) flux ratio middle 35th to middle 95th quantiles, (f) flux skew, (g) Butler & Bloom (2011) log(χ^2_{QSO}), and (h) Butler & Bloom (2011) log($\chi^2_{\mathrm{falseQSO}}$).

Table 3
Performance of Classifiers on OGLE+*Hipparcos* Data Set, Averaged over 10 Repetitions

Method	Misclassification %[a]	Catastrophic Error %[a]	CPU[b]
CART	32.2	13.7	10.6
C4.5	29.8	12.7	14.4
RF	**22.8**	8.0	117.6
Boost	25.0	9.9	466.5
CART.pw	25.8	8.7	323.2
RF.pw	23.4	8.0	290.3
Boost.pw	24.1	8.2	301.5
SVM.pw	25.3	8.4	273.0
HSC-RF	23.5	**7.8**	230.9
HMC–RF	23.4	8.2	946.0

Notes. Bold values denote the minimal error percentage.
[a] Estimated using 10-fold cross validation.
[b] Average processing time in seconds for 10-fold cross validation on a 2.67 GHz Macintosh with 4 GB of RAM.

can be generated for new data at the rate of 3700 instances per second.

4.3.1. Tree-based Classifiers

On average, the single-tree classifiers—CART and C4.5—are outperformed by the tree-ensemble methods–RF and tree boosting—by 21% in misclassification error rate. The classification performances of the single-tree classifiers are near that of the best classifier in Debosscher et al. (2007), which achieves a 30% error rate. Tree-based classifiers seem particularly adept at variable-star classification, and ensembles of trees achieve even better results. Single trees take on the order of 10 s to fit a model, prune based on cross-validation complexity, and predict classification labels for test cases. Tree-ensemble methods take 10–40 times longer to fit 1000 trees. Overall, the RF classifier is the best classification method for these data: it achieves the lowest overall misclassification rate, low catastrophic error rate, and is the third fastest algorithm. We compare single trees to a simple K-nearest neighbors classifier (KNN), which predicts the class of each variable star by polling its K closest counterparts in feature space. KNN dominates the single-tree classifiers in terms of both error rate and computational speed. We find that for this data, $K = 7$ is optimal, with the caveat that only the 25 features with highest RF variable importance be used; if all features are included, the best KNN error rate jumps to 37.5%.

4.3.2. Pairwise Classifiers

We implement four pairwise classifiers: CART, RF, boosted trees, and SVM. Of these, RF achieves the best results in terms of both misclassification rate and catastrophic error rate, at 23.4% and 8.0%, respectively. The pairwise classifiers all perform better than single-tree classifiers but tend to fare worse than the single RF method. It is interesting to note that our implementation of SVM achieves a 25.3% misclassification rate, a vast improvement over the 50% SVM misclassification rate found by Debosscher et al. (2007). This is likely due to both our use of better features and our pre-selection of the 25 features (chosen via cross validation) with highest RF variable importance for use in the SVM. Unlike tree models, SVM is not immune to the inclusion of many useless features; when we include all 53 features into the SVM, our error rate skyrockets to 54%.

4.3.3. Hierarchical Classifiers

Two of our classifiers, HSC–RF and HMC–RF, incorporate the hierarchical class taxonomy when building a classifier. Both of these methods achieve overall classification error rates slightly worse (sub-1% level) than that of the RF classifier, while HSC–RF reaches the best overall catastrophic error rate (7.8%). HMC–RF slightly outperforms HSC–RF with respect to misclassification rate, but its current implementation takes four times as much CPU time. HSC–RF, HMC–RF, pairwise RF, and the original RF are the best methods in terms of error rates, but RF is at least twice as fast as any of the other methods.

4.4. Direct Comparison to Debosscher et al. (2007)

RF achieves a 22.8% average misclassification rate, a 24% improvement over the 30% misclassification rate achieved by the best method of Debosscher et al. (2007; Bayesian model averaging of artificial neural networks). Furthermore, each of the classifiers proposed in this paper, except the single-tree models CART and C4.5, achieves an average misclassification rate smaller than 25.8% (see Table 3). There is no large discrepancy between the different ensemble methods—the difference between the best (RF) and worst (boosting) ensemble classifier is 2.2%, or an average of 34 more correct classifications—but in terms of both accuracy and speed, RF is the clear winner.

In comparing our results to the Debosscher et al. (2007) classification results, it is useful to know whether the gains in accuracy are due to the use of better classifiers, more accurate periodic-feature extraction, informative non-periodic features, or some combination of these. To this end, we classify these data using the following sets of features:

1. the periodic features estimated by Debosscher et al. (2007);
2. our estimates of the periodic features following Section 2;
3. the non-periodic features proposed in Section 2; and
4. the non-periodic features in addition to our periodic features.

Misclassification rates from the application of our classifiers to the above sets of features are plotted in Figure 4. As a general trend, using both our periodic and non-periodic features is better than using only our periodic features, which is in turn better than using Debosscher et al.'s periodic features, which achieves similar rates to using only the non-periodic features. Using an RF classifier, we find that the average cross-validated misclassification rates are 22.8% using all features, 23.8% using our periodic features, 26.7% using Debosscher et al. (2007) features, and 27.6% using only our non-periodic features. This is evidence that we obtain better classification results both because our classification model is better and because the extracted features we use are more informative.

4.5. Analysis of Classification Errors

Understanding the source and nature of the mistakes that our classifier makes can alert to possible limitations in the classification methods and feature-extraction software and aid in the construction of a second-generation light-curve classifier. Let us focus on the classifier with the best overall performance: the RF, whose cross-validated misclassification rate was 22.8%. In Figure 5, we plot the confusion matrix of this classifier, which is a tabular representation of the classifier's predicted class versus the true class. A perfect classifier would place all of the data on the diagonal of the confusion matrix; any deviations

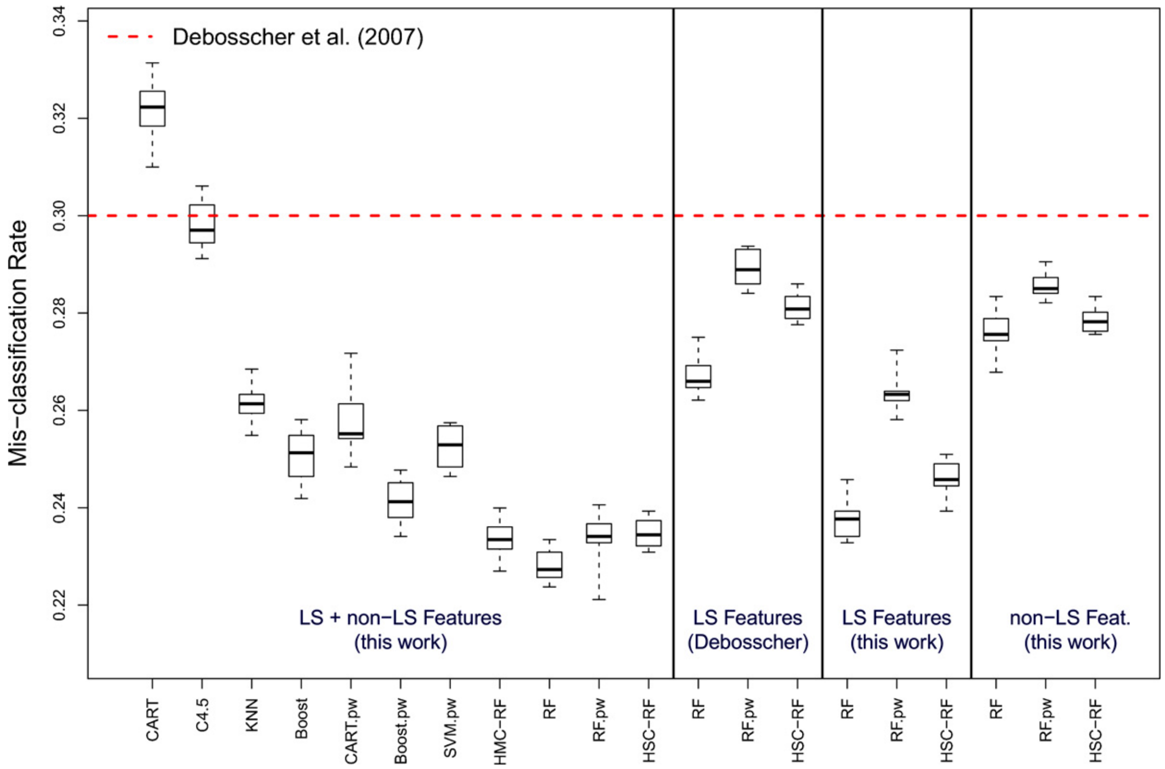

Figure 4. Distribution of cross-validation error rates for several classifiers on the OGLE+*Hipparcos* data, obtained from 10 repetitions. The classifiers are divided based on the features on which they were trained; from left to right: (1) all of the periodic and non-periodic features that we estimate, (2) the Lomb–Scargle features estimated by Debosscher et al. (2007), (3) the Lomb–Scargle features estimated by us, and (4) the non-periodic features. In terms of misclassification rate, the classifiers trained on all of our features perform the best, followed by those trained only on our periodic features, those trained on Debosscher et al.'s periodic features, and those trained on only the non-periodic features. All of the classifiers used, except single trees, achieve better error rates than the best classifier from Debosscher et al. (dashed line).

from the diagonal inform us of the types of errors that the classifier makes.

A few common errors are apparent in Figure 5. For instance, Lambda Bootis and Beta Cephei are frequently classified as Delta Scuti. Wolf-Rayet, Herbig AE/BE, and S Doradus stars are usually classified as Periodic Variable Super Giants, and T Tauri are often misclassified as Semiregular Pulsating Variables. None of these mistakes are particularly egregious: often the confused science classes are physically similar. Also, the misclassified examples often come from classes with few training examples (see below) or characteristically low-amplitude objects (see Section 4.8).

As the RF is a probabilistic classifier, for each source it supplies us with a probability estimate that the source belongs to each of the science classes. Until now, we have collapsed each vector of probabilities into an indicator of most probable class, but there is much information available to extract from the individual probabilities. For instance, in Figure 6 we plot, by class, the RF estimated probability that each source is of its true class. We immediately see a large disparity in performance between the classes: for a few classes, we estimate high probabilities of true class, while for others we generally estimate low probabilities. This discrepancy is related to the size of each class: within the science classes that are data-rich, we tend to get the correct class, while in classes with scarce data, we usually estimate the wrong class. This same effect is seen in Debosscher et al. (2007, their Table 5). This is a common problem in statistical classification for imbalanced class sizes: classifiers such as RF try to minimize the overall classification rate, thus focusing most of their efforts on the larger classes. In these methods, there is an implicit prior that the class frequencies equal their observed proportions. One can attempt to achieve better error rates within the smaller classes by imposing a flat prior, which is attained by weighting the training data inversely proportional to their class frequency. The price to pay for the increase in balanced error among the classes is a higher overall misclassification rate (see Breiman et al. 1984). The better solution is to obtain more training examples for the undersampled classes to achieve a better characterization of these sources.

We have experimented with an RF classifier using inverse class-size weighting. The results of this experiment were as expected: our overall misclassification rate climbs to 28.0%, a 23% increase in error over the standard RF, but we perform better within the smaller classes. Notably, the number of correctly classified Lambda Bootis increases from 1 to 7, while the number of correctly classified Ellipsoidal variables jumps from 6 to 11, Beta Cephei from 5 to 23, and Gamma Doradus from 8 to 15. All four classes in which the original RF found no correct classifications each had at least two correct classifications with the weighted RF.

4.6. Performance for Specific Science Classes

Although our classifier was constructed to minimize the number of overall misclassifications in the 25-class problem, we can also use it to obtain samples of objects from science classes of interest via probability thresholding. The RF classifier produces a set of classwise posterior probability estimates for each object. To construct samples of a particular science class, we define a threshold on the posterior probabilities, whereby any object with class probability estimate larger than the threshold is included in the sample. By decreasing the threshold, we trade-off

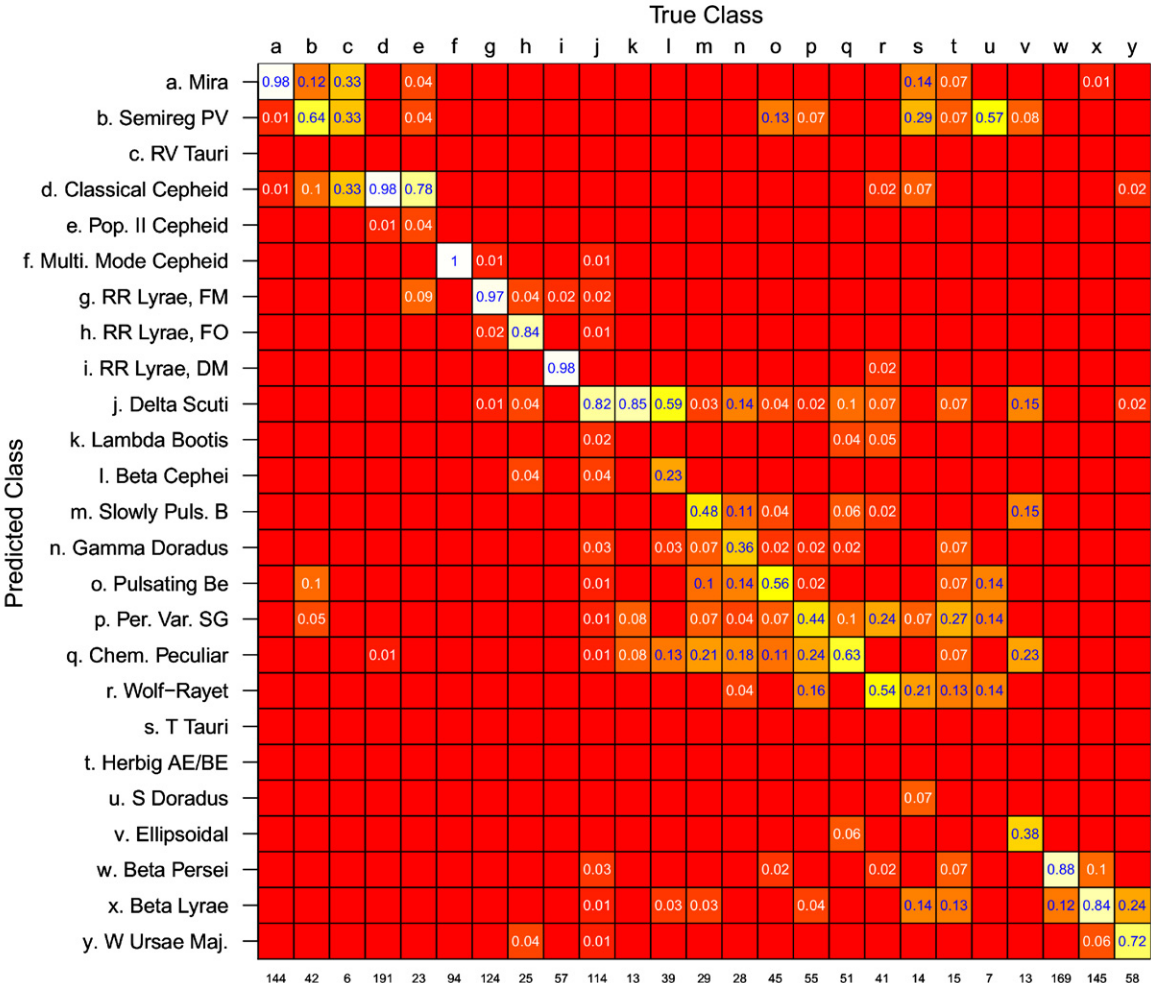

	a	b	c	d	e	f	g	h	i	j	k	l	m	n	o	p	q	r	s	t	u	v	w	x	y
a. Mira	0.98	0.12	0.33		0.04														0.14	0.07				0.01	
b. Semireg PV	0.01	0.64	0.33		0.04										0.13	0.07			0.29	0.07	0.57	0.08			
c. RV Tauri																									
d. Classical Cepheid	0.01	0.1	0.33	0.98	0.78													0.02	0.07						0.02
e. Pop. II Cepheid				0.01	0.04																				
f. Multi. Mode Cepheid						1	0.01			0.01															
g. RR Lyrae, FM					0.09		0.97	0.04	0.02	0.02															
h. RR Lyrae, FO							0.02	0.84		0.01															
i. RR Lyrae, DM									0.98									0.02							
j. Delta Scuti							0.01	0.04		0.82	0.85	0.59	0.03	0.14	0.04	0.02	0.1	0.07		0.07		0.15			0.02
k. Lambda Bootis										0.02							0.04	0.05							
l. Beta Cephei								0.04		0.04		0.23													
m. Slowly Puls. B													0.48	0.11	0.04		0.06	0.02				0.15			
n. Gamma Doradus										0.03		0.03	0.07	0.36	0.02	0.02	0.02			0.07					
o. Pulsating Be		0.1								0.01			0.1	0.14	0.56	0.02				0.07	0.14				
p. Per. Var. SG		0.05								0.01	0.08		0.07	0.04	0.07	0.44	0.1	0.24	0.07	0.27	0.14				
q. Chem. Peculiar				0.01						0.01	0.08	0.13	0.21	0.18	0.11	0.24	0.63			0.07		0.23			
r. Wolf−Rayet														0.04		0.16		0.54	0.21	0.13	0.14				
s. T Tauri																									
t. Herbig AE/BE																									
u. S Doradus																			0.07						
v. Ellipsoidal																	0.06					0.38			
w. Beta Persei										0.03					0.02			0.02		0.07			0.88	0.1	
x. Beta Lyrae										0.01		0.03	0.03			0.04			0.14	0.13			0.12	0.84	0.24
y. W Ursae Maj.								0.04		0.01														0.06	0.72
	144	42	6	191	23	94	124	25	57	114	13	39	29	28	45	55	51	41	14	15	7	13	169	145	58

Figure 5. Cross-validated confusion matrix obtained by the random forest classifier for the OGLE+*Hipparcos* data. A perfect classifier would place all mass on the diagonal. We have sorted the science classes by physical similarity, so large numbers near the diagonal signify that the classifier is performing well. On average, the classifier performs worse on the eruptive events, as exemplified by a large spread of mass for classes *p* through *u*. The overall error rate for this classifier was 21.1%.

purity of the sample for completeness, thereby mapping out the receiver operating characteristic (ROC) curve of the classifier.

In Figure 7, we plot the cross-validated ROC curve of the multi-class RF for four different science classes: (a) RR Lyrae, FM, (b) T Tauri, (c) Milky Way Structure, which includes all Mira, RR Lyrae, and Cepheid stars, and (d) Eclipsing Systems, which include all Beta Persei, Beta Lyrae, and W Ursae Major stars. Each ROC curve shows the trade-off between the efficiency and purity of the samples. At a 95% purity, the estimated efficiency for RR Lyrae, FM, is 94.7%, for Milky Way Structure stars 98.2%, and for Eclipsing Systems 99.1%. The T Tauri ROC curve is substantially worse than these other classes due to the small number of sources (note: inverse class-size weighting does not help in this problem because the ordering of the posterior class probabilities drives the ROC curve, not the magnitude of those probabilities). Surprisingly, the 25-class RF ROC curve dominates the ROC curve of a one-versus-all RF for three of the four science classes, with vastly superior results for small classes.

4.7. *Feature Importance*

In Section 3.2, we described how to estimate the importance of each feature in a tree-based classifier. In Figure 8, the importance of each feature from a pairwise RF classifier is plotted by class. The intensity of each pixel depicts the proportion of instances of each class that are correctly classified by using each particular feature in lieu of a feature containing random noise. The intensities have been scaled to have the same mean across classes to mitigate the effects of unequal class sizes and are plotted on a square-root scale to decrease the influence of dominant features. In independently comparing the performance of each feature to that of noise, the method does not account for correlations among features. Consequentially, sets of features that measure similar properties—e.g., `median_absolute_deviation`,`std`,and `stetson_j` are all measures of the spread in the fluxes—may each have high importance, even though their combined importance is not much greater than each of their individual importances.

Figure 8 shows that a majority of the features used in this work have substantial importance in the RF classifier for discerning at least one science class. Close inspection of this figure illuminates the usefulness of certain features for distinguishing specific science classes. As expected, the amplitude and frequency of the first harmonic, along with the features related to the spread and skew of the flux measurements, have the highest level of importance. The flux amplitude is particularly important for classifying Mira stars, Cepheids, and RR Lyrae, which are distinguished by their large amplitudes. The frequency of the first harmonic has high importance for most pulsating stars, likely because these classes have similar amplitudes but

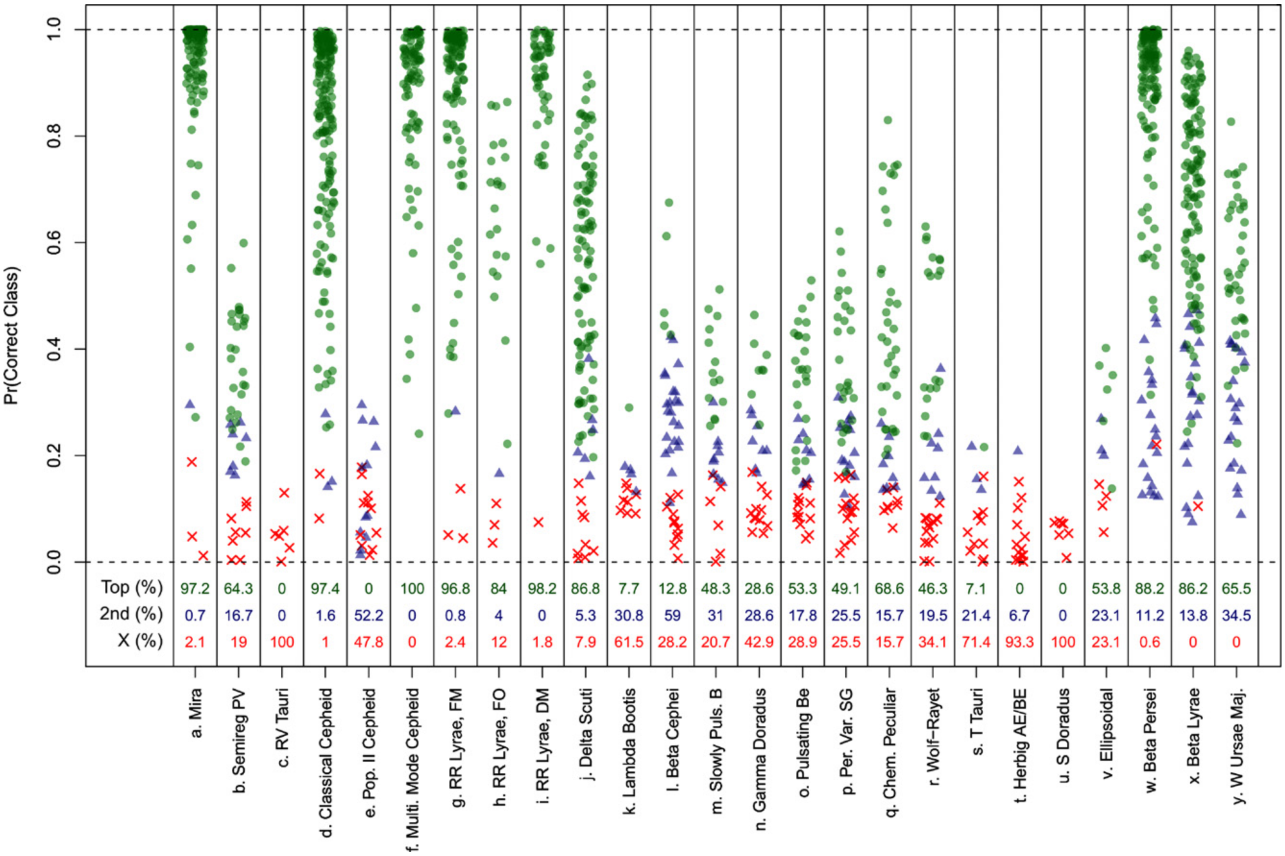

Figure 6. Cross-validated random forest probability estimate of the correct class for each variable star, plotted by class. Green circles indicate that the classifier's top choice for that object was correct, blue triangles indicate that the second choice was correct, and red "×"s indicated that neither of the top two were correct. As a general trend, we find that the classifier performs better for large classes.

different frequencies. The QSO-variability feature is important for identifying eruptive sources, such as Periodically Variable Super Giants and Chemically Peculiar stars, because these stars generally have small values of the QSO feature compared to other variable star classes.

In addition, there are several features that have very low importance for distinguishing any of the science classes. These features include the relative phase offsets for each of the harmonics, the amplitudes of the higher-order harmonics, and non-periodic features such as `beyond1std`, `max_slope`, and `pair_slope_trend`. We rerun the RF classifier excluding the 14 features with the smallest feature importance (the excluded features are nine relative phase offsets, `beyond1std`, `max_slope`, `pair_slope_trend`, and the 65th, and 80th middle flux percentiles. Results show a cross-validated error rate of 22.8% and a catastrophic error rate of 8.2% (averaged over 10 repetitions of the RF), which is consistent with the error rates of the RF trained on all 53 features, showing the insensitivity of the RF classifier to inclusion of features that carry little or no classification information.

4.8. Classification of High-amplitude (>0.1 mag) Sources

High-amplitude variable stars constitute many of the central scientific impetuses of current and future surveys. In particular, finding and classifying pulsational variables with known period–luminosity relationships (Mira, Cepheids, and RR Lyrae) is a major thrust of the LSST (Walkowicz et al. 2009; LSST Science Collaborations et al. 2009). Moreover, light curves from low-amplitude sources generally have a lower S/N, making it more difficult to estimate their light-curve-derived features and hence more difficult to obtain accurate classifications. Indeed, several of the classes in which we frequently make errors are populated by low-amplitude sources.

Here we classify only those light curves with amplitudes greater than 0.1 mag, removing low-amplitude classes from the sample. This results in the removal of 383 sources, or 25% of the data. After excluding these sources, we are left with a handful of classes with less than seven sources. Due to the difficulty in training (and cross validating) a classifier for classes with such small amount of data, we ignore those classes, resulting in the exclusion of 19 more sources, bringing the total to 408 excluded sources, or 26% of the entire data set. We are left with 1134 sources in 16 science classes.

On this subset of data, our RF classifier achieves a cross-validated misclassification rate of 13.7%, a substantial improvement from the 22.8% misclassification rate from the best classifier on the entire data set. The catastrophic misclassification rate is only 3.5%, compared to 8.0% for the entire data set. In Figure 9, the confusion matrix for the classifier is plotted. The most prevalent error is misclassifying Pulsating Be and T Tauri stars as semiregular pulsating variables. On average eight of the nine Pulsating Be stars and four of the twelve T Tauri stars are misclassified as semiregular pulsating variables.

4.9. OGLE versus Hipparcos

Data for the sources that we classify in this section come from either the OGLE or *Hipparcos* surveys. Specifically, there are 523 sources from five science classes whose data are from

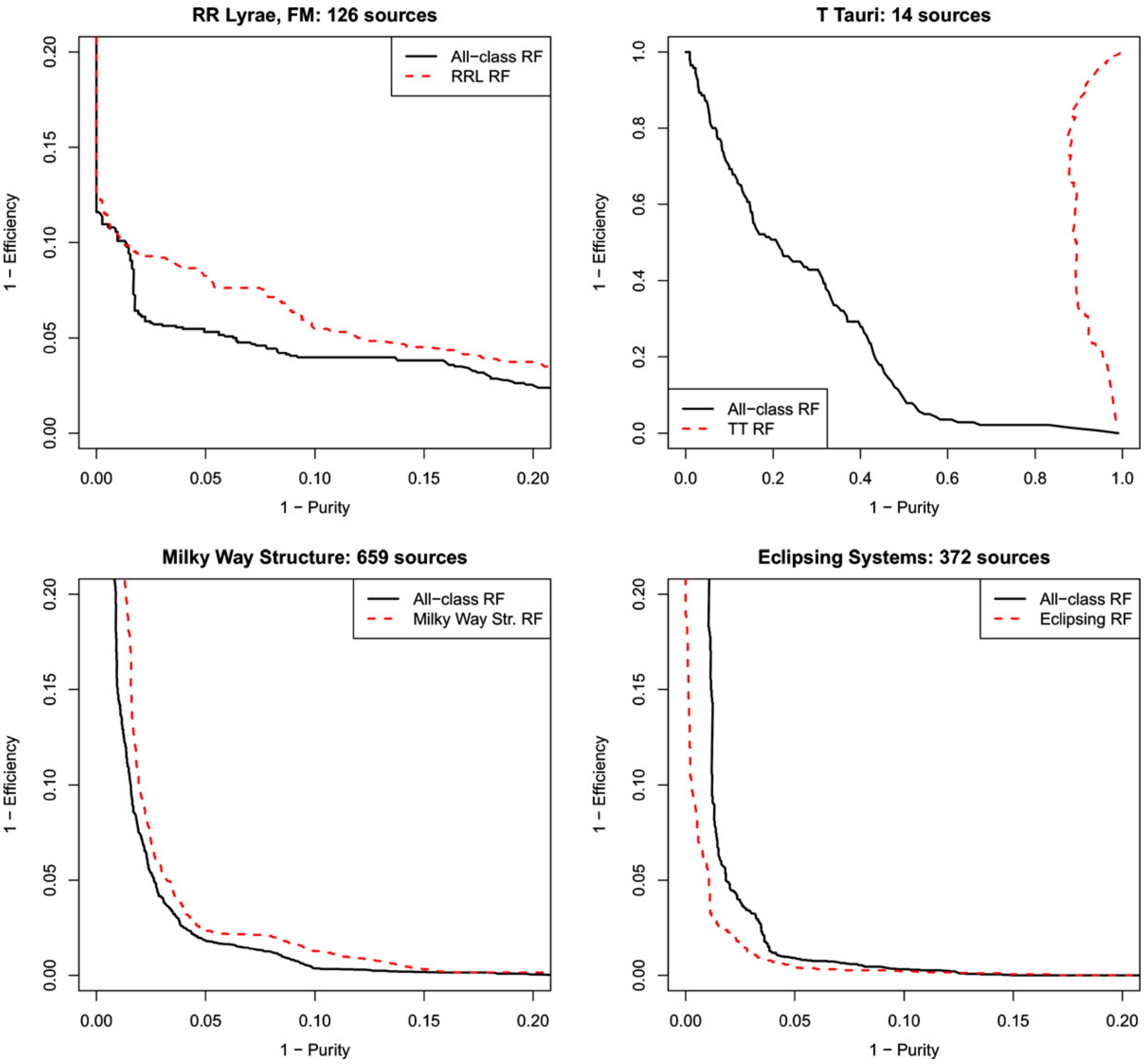

Figure 7. Cross-validated ROC curves, averaged over 10 cross-validation trials, for four different science classes: (a) RR Lyrae, FM, (b) T Tauri, (c) Milky Way Structure, which includes all Mira, RR Lyrae, and Cepheid stars, and (d) Eclipsing Systems, which includes all Beta Persei, Beta Lyrae, and W Ursae Major stars. Plotted is 1-Efficiency vs. 1-Purity as a function of the class threshold. The 25-class random forest ROC curve (solid black line) dominates the ROC curve of a one-versus-all random forest (dashed red line) for each science class except Eclipsing Systems. For T Tauri, the all-class random forest is vastly superior to the T Tauri-specific classifier.

OGLE, while the data from the remaining 858 sources are from *Hipparcos*. Our classifiers tend to perform much better for the OGLE data than for the *Hipparcos* sources: for the RF classifier we obtain a 11.3% error rate for OGLE data and 27.9% error rate for *Hipparcos*.

It is unclear whether the better performance for OGLE data is due to the relative ease at classifying the five science classes with OGLE data or because of differences in the survey specifications. The sampling rate of the OGLE survey is three times higher than that of *Hipparcos*. The average number of observations per OGLE source is 329, compared to 103 for *Hipparcos*, even though the average time baselines for the surveys are each near 1100 days. OGLE observations have on average twice the flux as *Hipparcos* observations, but the flux measurement errors of OGLE light curves tend to be higher, making their respective S/Ns similar (OGLE flux measurements have on average an S/N 1.25 times higher than *Hipparcos* S/Ns).

To test whether the observed gains in accuracy between OGLE and *Hipparcos* sources are due to differences in the surveys or differences in the science classes observed by each survey, we run the following experiment. For each OGLE light curve, we thin the flux measurements down to one-third of the original observations to mimic *Hipparcos* conditions and rerun the feature-extraction pipeline and classifier using the thinned light curves. Note that we do not add noise to the OGLE data because of the relative similarity in average S/N between the surveys; the dominant difference between data of the two surveys is the sampling rate. Results of the experiment are that the error rate for OGLE data increases to 13.0%, an increase of only 1.7% representing nine more misclassified OGLE sources. This value remains much lower than the *Hipparcos* error rate, showing that the better classifier performance for OGLE data is primarily driven by the ease of distinguishing those science classes.

5. CONCLUSIONS AND FUTURE WORK

We have presented a thorough study of automated variable-star classification from sparse and noisy single-band light curves. In the 25-class problem considered by Debosscher et al.

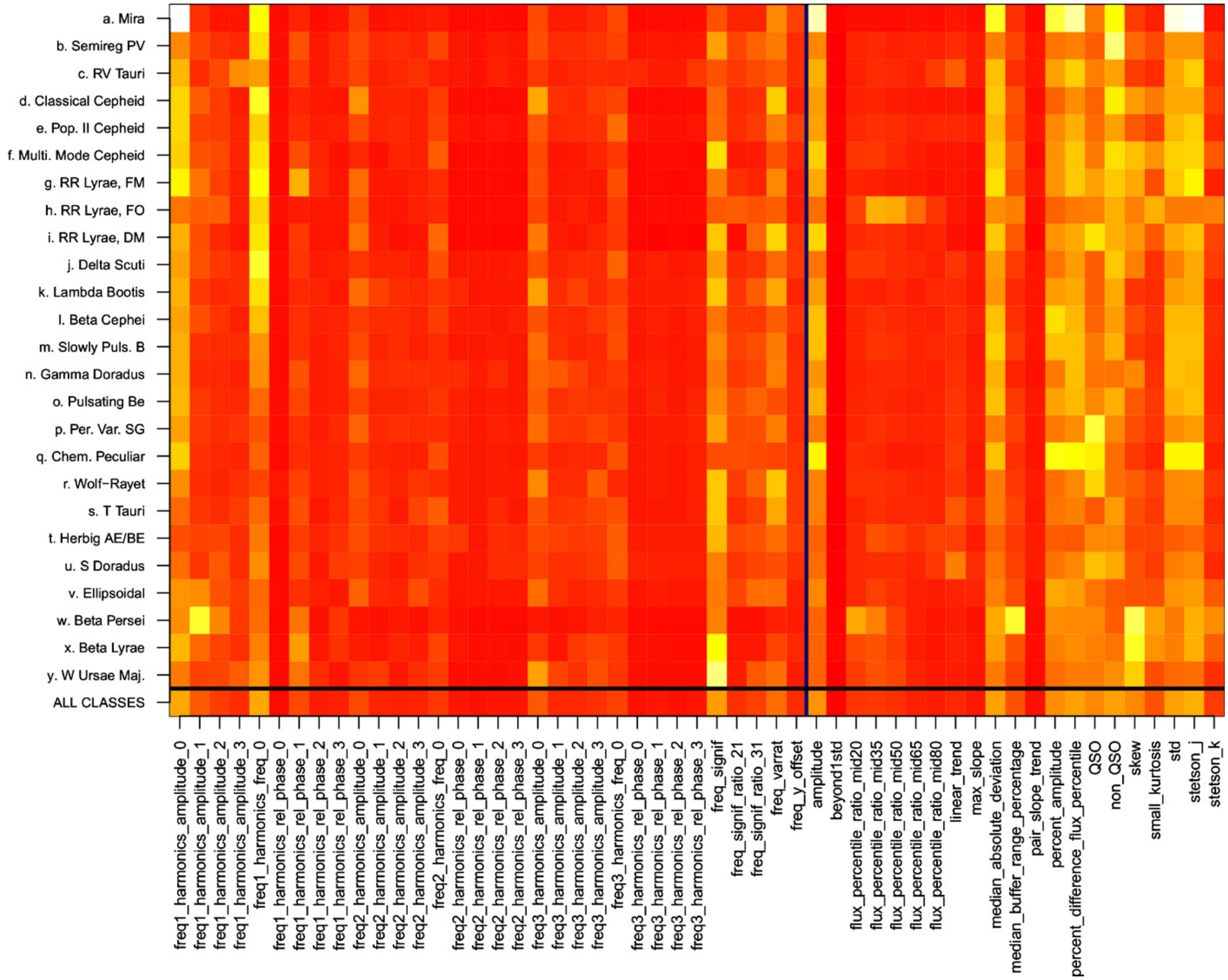

Figure 8. Pairwise random forest feature importance. Intensity is the square root of the proportion of instances of each class classified correctly because of that feature (compared to a replacement random permutation of that feature). Features are split into periodic (left) and non-periodic (right) features. The periodic features related to the first frequency are the most important, with higher-order frequencies and harmonics having smaller importance. The non-periodic features related to spread and skew have high importance in the classifier, as do the QSO-variability features.

(2007), which includes all of the most important variable-star science classes, we obtain a 24% improvement over their best classifier in terms of misclassification error rate. We attribute this improvement to all of the following advances.

1. *More accurate periodic-feature estimation.* Our Lomb–Scargle period-fitting code is both fast and accurate. With the same RF classifier, the average error rate using our periodic-feature estimates is 23.8%, compared to an error rate of 26.7% using only Debosscher's period feature estimates, representing an improvement of 11%.
2. *Use of predictive non-periodic features.* Simple summary statistics and more sophisticated model parameters give a significant improvement. Using both our periodic and non-periodic features, the RF error rate is 22.8%, a 4% improvement over using only our periodic features.
3. *Better classification methods.* The classifiers that we use are more flexible and more well suited for multi-class variable-star classification. All of the methods considered in this paper, save the single-tree models, achieve a statistically significant improvement over Debosscher's best classifier. Our RF classifier, applied to the exact features used by that paper, achieves an 11% improvement over their best error rate, 30%.

We have shown the adeptness of tree-based classifiers in the problem of variable-star classification. We demonstrated the superiority of the RF classifier in terms of error rates, speed, and immunity to features with little useful classification information. We outlined how to calculate the optimal probability threshold to obtain pure and complete samples of specified subclasses and showed that the multi-class RF is often superior to the one-versus-all RF in this problem. We advocate the continued use of this method for other classification problems in astronomy.

Furthermore, we described how the RF classifier can be used to estimate the importance of each feature by computing the expected classification gains versus replacing that feature with random noise. In the variable-star classification problem, it was found that several non-periodic features have high importance. A classifier built only on the non-periodic features still performs quite well, attaining 27.6% error rate.

Finally, this paper is the first to use the known variable-star taxonomy both to train a classifier and evaluate its result. We introduced two different classification methods to incorporate a

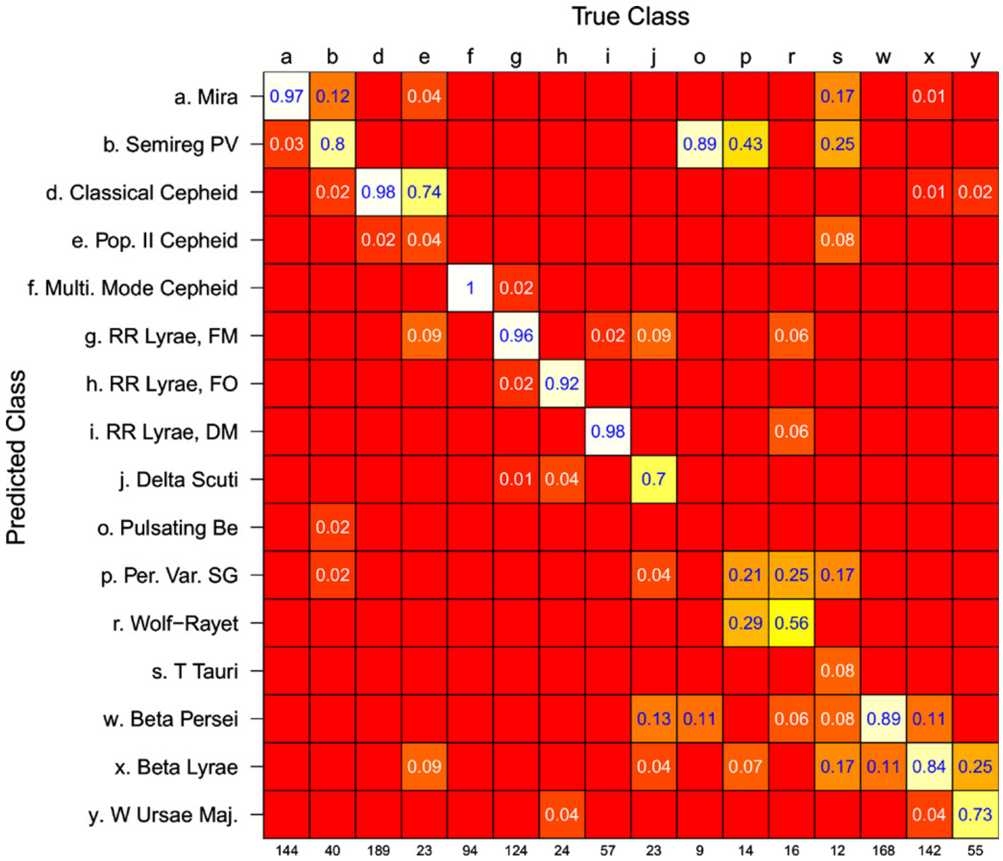

	a	b	d	e	f	g	h	i	j	o	p	r	s	w	x	y
a. Mira	0.97	0.12		0.04									0.17		0.01	
b. Semireg PV	0.03	0.8								0.89	0.43		0.25			
d. Classical Cepheid		0.02	0.98	0.74											0.01	0.02
e. Pop. II Cepheid			0.02	0.04									0.08			
f. Multi. Mode Cepheid					1	0.02										
g. RR Lyrae, FM				0.09		0.96		0.02	0.09			0.06				
h. RR Lyrae, FO						0.02	0.92									
i. RR Lyrae, DM								0.98				0.06				
j. Delta Scuti						0.01	0.04		0.7							
o. Pulsating Be		0.02														
p. Per. Var. SG		0.02							0.04		0.21	0.25	0.17			
r. Wolf−Rayet											0.29	0.56				
s. T Tauri													0.08			
w. Beta Persei									0.13	0.11		0.06	0.08	0.89	0.11	
x. Beta Lyrae				0.09					0.04		0.07		0.17	0.11	0.84	0.25
y. W Ursae Maj.							0.04								0.04	0.73
	144	40	189	23	94	124	24	57	23	9	14	16	12	168	142	55

Figure 9. Cross-validated confusion matrix for a random forest classifier applied only to the OGLE+*Hipparcos* sources with amplitude greater than 0.1 mag. The overall error rate for this subset of data is 13.7%, with catastrophic misclassification rate of 3.5%.

hierarchical taxonomy: HSC, which builds a different classifier in each non-terminal node of the taxonomy, and HMC, which fits a single classifier, penalizing errors at smaller depths in the taxonomy more heavily. We demonstrated that both of these methods perform well, in terms of classification rate and catastrophic error rate. The class taxonomy was also used to introduce the notion of catastrophic error rate, which considers as catastrophic any error made at the top level of the hierarchy.

Several open questions remain with regard to the automated classification of astronomical time series. Many of these questions will be addressed by us in future publications, where we will expand on the methodology presented here and attempt to classify data from other surveys, such as the All Sky Automated Survey (ASAS), SDSS Stripe 82, *Kepler*, and the Wide Angle Search for Planets (WASP). Some of the questions that we will address are the following.

1. If we train a classifier on a set of objects from one (or multiple) survey(s), will that classifier be appropriate to predict the classes of objects from the new survey? This question is of great importance because presumably a set of known (labeled) variable stars will be compiled from previous surveys to train a classifier for use on a new survey.
2. What features are robust across a wide range of different surveys, each with different cadences? If some sets of features are robust to survey design and cadence, those should be used in lieu of survey-dependent features in a classifier. In this paper, we have excluded any feature that was blatantly survey dependent (such as the Welch–Stetson variability index *I*, which uses mean flux), but this does not guarantee that some features will not have survey dependence.
3. How does mislabeled training data affect the classifier accuracy? Can mislabeled data be effectively detected and cleaned from the classification set?
4. How can a classifier be trained to efficiently identify outliers/new types of variables? Future surveys will unquestionably discover new science classes that do not fit under any of the training classes. Recent studies by, e.g., Protopapas et al. (2006) and Rebbapragada et al. (2009), have searched for outliers in variable-star catalogs. Methodology has also been developed recently in the statistics and machine-learning literature for outlier discovery in large time-series databases (Yankov et al. 2008).
5. How are the error rates of a classifier affected by computational limitations (where, perhaps some CPU-intensive or external server-dependent features are not used)? In automated classification of astronomical sources, there is often a time sensitivity for follow-up observations. Presumably, there are more useful features for classification than the ones that we employed in this paper, but they may be expensive to compute or retrieve for each observation. This trade-off between error rate and computation time must be explored.

Finally, as a longer-term goal, we are striving to develop methodology that can be used on an LSST-caliber survey. This means that our methods must be fast enough to compute features and class probabilities for thousands of objects per night, work well at an LSST cadence, be applicable to multi-band light curves, and perform classification for all types of astronomical

Table 4
Periodic Features Extracted from Light Curves Using Generalized Lomb–Scargle

Feature	Description[a]
`freq1_harmonics_amplitude_0`	$A_{1,1}$[b]
`freq1_harmonics_amplitude_1`	$A_{1,2}$
`freq1_harmonics_amplitude_2`	$A_{1,3}$
`freq1_harmonics_amplitude_3`	$A_{1,4}$
`freq1_harmonics_freq_0`	f_1[c]
`freq1_harmonics_rel_phase_0`	$\mathrm{PH}_{1,1}$[d]
`freq1_harmonics_rel_phase_1`	$\mathrm{PH}_{1,2}$
`freq1_harmonics_rel_phase_2`	$\mathrm{PH}_{1,3}$
`freq1_harmonics_rel_phase_3`	$\mathrm{PH}_{1,4}$
`freq2_harmonics_amplitude_0`	$A_{2,1}$
`freq2_harmonics_amplitude_1`	$A_{2,2}$
`freq2_harmonics_amplitude_2`	$A_{2,3}$
`freq2_harmonics_amplitude_3`	$A_{2,4}$
`freq2_harmonics_freq_0`	f_2
`freq2_harmonics_rel_phase_0`	$\mathrm{PH}_{2,1}$
`freq2_harmonics_rel_phase_1`	$\mathrm{PH}_{2,2}$
`freq2_harmonics_rel_phase_2`	$\mathrm{PH}_{2,3}$
`freq2_harmonics_rel_phase_3`	$\mathrm{PH}_{2,4}$
`freq3_harmonics_amplitude_0`	$A_{3,1}$
`freq3_harmonics_amplitude_1`	$A_{3,2}$
`freq3_harmonics_amplitude_2`	$A_{3,3}$
`freq3_harmonics_amplitude_3`	$A_{3,4}$
`freq3_harmonics_freq_0`	f_3
`freq3_harmonics_rel_phase_0`	$\mathrm{PH}_{3,1}$
`freq3_harmonics_rel_phase_1`	$\mathrm{PH}_{3,2}$
`freq3_harmonics_rel_phase_2`	$\mathrm{PH}_{3,3}$
`freq3_harmonics_rel_phase_3`	$\mathrm{PH}_{3,4}$
`freq_signif`	Significance of f_1 versus null hypothesis of white noise with no periodic variation, computed using a Student's-T distribution
`freq_signif_ratio_21`	Ratio of significance of f_2 versus null to f_1 versus null
`freq_signif_ratio_31`	Ratio of significance of f_3 versus null to f_1 versus null
`freq_varrat`	Ratio of the variance after to the variance before subtraction of the fit with f_1 and its four harmonics
`freq_y_offset`	c

Notes.
[a] Notation from the discussion of Lomb–Scargle periodic-feature extraction in Section 2.1 is used.
[b] All amplitudes are in units of magnitude.
[c] All frequencies are in units of cycles day^{-1}.
[d] All relative phases are unitless ratios.

objects, including transients, variable stars, and QSOs. Our task, looking forward, is to address each of these problems and develop methodology for fast and accurate classification for LSST.

The authors acknowledge the generous support of a Cyber-Enabled Discovery and Innovation (CDI) grant (No. 0941742) from the National Science Foundation. This work was performed in the CDI-sponsored Center for Time Domain Informatics (http://cftd.info). N.R.B. is supported through the Einstein Fellowship Program (NASA Cooperative Agreement: NNG06DO90A). J.S.B. and D.L.S. also thank the Las Cumbres Observatory for support during the early stages of this work. We acknowledge helpful conversations with Dovi Poznanski, Tim Brown, John Rice, Noureddine El Karoui, James Long, Martin Wainwright, Elizabeth Purdom, Tamas Budavari, Kirk Borne, and Jeff Scargle. We thank J. Debosscher for assistance in obtaining the data from his paper.

The light-curve data and estimated features used in this paper can be retrieved from http://lyra.berkeley.edu/jwrichar/varStarClass_ApJ_data.tar.gz. Light curves are also accessible from http://dotastro.org.

APPENDIX A

FEATURES ESTIMATED FROM LIGHT CURVES

A description of the 32 periodic features computed using the methodology in Section 2.1 is in Table 4. In addition to these 32 periodic features, we calculate 20 non-periodic features for every light curve (Section 2.2). These features are compiled in Table 5. These consist primarily of simple statistics that can be calculated in the limit of few data points and also when no period is known in order to characterize the flux variation distribution. Where possible, we give the name of the Python function that calculates the feature (e.g., skewness is from `scipy.stats.skew()` in the Python SciPy module).

We begin with basic moment calculations using the observed photometric magnitude *mag* vector for each source:

1. `skew`: skewness of the magnitudes: scipy.stats.skew();
2. `small_kurtosis`: small sample kurtosis of the magnitudes;[10]

[10] See http://www.xycoon.com/peakedness_small_sample_test_1.htm.

Table 5
Non-periodic Features Extracted from Light Curves

Feature	Description
amplitude	Half the difference between the maximum and the minimum magnitude
beyond1std	Percentage of points beyond one st. dev. from the weighted mean
flux_percentile_ratio_mid20	Ratio of flux percentiles (60th–40th) over (95th–5th)
flux_percentile_ratio_mid35	Ratio of flux percentiles (67.5th–32.5th) over (95th–5th)
flux_percentile_ratio_mid50	Ratio of flux percentiles (75th–25th) over (95th–5th)
flux_percentile_ratio_mid65	Ratio of flux percentiles (82.5th–17.5th) over (95th–5th)
flux_percentile_ratio_mid80	Ratio of flux percentiles (90th–10th) over (95th–5th)
linear_trend	Slope of a linear fit to the light-curve fluxes
max_slope	Maximum absolute flux slope between two consecutive observations
median_absolute_deviation	Median discrepancy of the fluxes from the median flux
median_buffer_range_percentage	Percentage of fluxes within 20% of the amplitude from the median
pair_slope_trend	Percentage of all pairs of consecutive flux measurements that have positive slope
percent_amplitude	Largest percentage difference between either the max or min magnitude and the median
percent_difference_flux_percentile	Diff. between the 2nd and 98th flux percentiles, converted to magnitude[a]
QSO	Quasar variability metric in Butler & Bloom (2011), $\log(\chi^2_{\rm QSO})$
non_QSO	Non-quasar variability metric in Butler & Bloom (2011), $\log(\chi^2_{\rm falseQSO})$
skew	Skew of the fluxes
small_kurtosis	Kurtosis of the fluxes, reliable down to a small number of epochs
std	Standard deviation of the fluxes
stetson_j	Welch–Stetson variability index J[b]
stetson_k	Welch–Stetson variability index K[b]

Notes.
[a] Eyer (2005).
[b] Stetson (1996).

3. std: standard deviation of the magnitudes: Numpy std();
4. beyond1std: the fraction ($\leqslant$1) of photometric magnitudes that lie above or below one std() from the weighted (by photometric errors) mean;
5. stetson_j: Stetson (1996) variability index, a robust standard deviation;
6. stetson_k: Stetson (1996) robust kurtosis measure.

We also calculate the following basic quantities using the magnitudes:

1. max_slope: examining successive (time-sorted) magnitudes, the maximal first difference (value of delta magnitude over delta time);
2. amplitude: difference between the maximum and minimum magnitudes;
3. median_absolute_deviation: median($|mag$ − median $(mag)|$);
4. median_buffer_range_percentage: fraction ($\leqslant$1) of photometric points within amplitude/10 of the median magnitude;
5. pair_slope_trend: considering the last 30 (time-sorted) measurements of source magnitude, the fraction of increasing first differences minus the fraction of decreasing first differences.

We also characterize the sorted flux $F = 10^{-0.4\,{\rm mag}}$ distribution using percentiles, following Eyer (2006). If $F_{5,95}$ is the difference between 95% and 5% flux values, we calculate the following:

1. flux_percentile_ratio_mid20: ratio $F_{40,60}/F_{5,95}$;
2. flux_percentile_ratio_mid35: ratio $F_{32.5,67.5}/F_{5,95}$;
3. flux_percentile_ratio_mid50: ratio $F_{25,75}/F_{5,95}$;
4. flux_percentile_ratio_mid65: ratio $F_{17.5,82.5}/F_{5,95}$;
5. flux_percentile_ratio_mid80: ratio $F_{10,90}/F_{5,95}$;
6. percent_amplitude: the largest absolute departure from the median flux, divided by the median flux;
7. percent_difference_flux_percentile: ratio of $F_{5,95}$ over the median flux.

Finally, useful for stochastically varying sources, we calculate the quasar similarity metrics from Butler & Bloom (2011):

1. QSO: quality of fit $\chi^2_{\rm QSO}/\nu$ for a quasar-like source, assuming mag = 19;
2. non_QSO: quality of fit for a non-quasar-like source (related to NULL value of QSO).

APPENDIX B

DOUBLY LABELED STARS

As discussed in Section 4.1, there are 25 sources with more than one class label. Five of these objects are labeled as both S Doradus and periodically variable super giants. We assign these to the S Doradus class because S Doradus is a subclass of periodically variable super giants. Two other sources, V* BF Ori and HD 97048, were verified to be Herbig AE/BE-type stars by Grinin et al. (2010) and Doering et al. (2007), respectively. RY Lep is listed incorrectly in Simbad as an Agol-type eclipsing system (its original 50 year old classification) and as RR Lyrae/Delta Scuti. Derekas et al. (2009) clearly establish this source as a high-amplitude δ-Scuti in a binary system. Likewise, HIP 99252 is a δ-Scuti star (Rodríguez et al. 2000) and not also an RR Lyrae. HIP 30326 (=V Mon) is a Mira variable and not also part of the RV Tauri class (Whitelock et al. 2008). HD 210111 (listed also as delta Scuti) is a λ Bootis star (Paunzen & Reegen 2008). HD 165763 is a W-R star that is not periodic to a high degree of confidence (Moffat et al. 2008). Likewise, WR40 is not periodic as it was once believed (Marchenko et al. 1994). We found no reference to the periodic nature of the W-R star HD 156385. The remaining 11 sources were of ambiguous class or truly deserved of two classes and were excluded from the training and testing sample. These stars are listed in Table 6 and briefly mentioned below.

Table 6
Doubly Labeled Sources Excluded from the Sample for Both Training and Testing Purposes

R.A.	Decl.	ID	Class 1[a]	Class 2[a]	RF Best Class [b]	RF 2nd Best Class [c]
05 26 50.2284	+03 05 44.428	HD 35715	l. Beta Cephei	v. Ellipsoidal	m. Slowly Puls. B (0.214)	v. Ellipsoidal (0.164)
05 36 06.2333	−07 23 47.320	HD 37151	q. Chem. Peculiar	m. Slowly Puls. B	p. Per. Var. SG (0.211)	n. Gamma Doradus (0.155)
06 54 13.0441	−23 55 42.011	HD 50896	r. Wolf-Rayet	p. Per. Var. SG	v. Ellipsoidal (0.181)	o. Pulsating Be (0.145)
07 03 43.1619	−11 33 06.209	HIP 34042	t. Herbig AE/BE	s. T Tauri	b. Semireg PV (0.287)	d. Classical Cepheid (0.114)
07 33 31.7288	+47 48 09.823	TV Lyn	j. Delta Scuti	h. RR Lyrae, FO	h. RR Lyrae, FO (0.686)	g. RR Lyrae, FM (0.12)
07 58 58.8801	+72 47 15.411	UY Cam	j. Delta Scuti	h. RR Lyrae, FO	h. RR Lyrae, FO (0.236)	j. Delta Scuti (0.222)
10 56 11.5763	−60 27 12.815	HD 94910	r. Wolf-Rayet	u. S Doradus	b. Semireg PV (0.258)	a. Mira (0.243)
11 51 15.3088	−55 48 15.795	V753 Cen	j. Delta Scuti	h. RR Lyrae, FO	h. RR Lyrae, FO (0.469)	j. Delta Scuti (0.151)
12 04 47.2738	−27 40 43.295	IK Hya	e. Pop. II Cepheid	g. RR Lyrae, FM	g. RR Lyrae, FM (0.456)	y. W Ursae Maj. (0.100)
15 24 11.3087	−62 40 37.567	HD 136488	p. Per. Var. SG	r. Wolf-Rayet	r. Wolf-Rayet (0.161)	p. Per. Var. SG (0.147)
21 04 32.9211	+50 47 03.276	V1719 Cyg	j. Delta Scuti	h. RR Lyrae, FO	j. Delta Scuti (0.315)	y. W Ursae Maj. (0.226)

Notes.
[a] Classes determined by Debosscher et al. (2007).
[b] Most likely class determined by a random forest classifier. Posterior probability in parentheses.
[c] Second-best candidate class determined by a random forest classifier. Posterior probability in parentheses.

1. *HD 136488 = HIP 75377*. This is a W-R with a measured periodicity in *Hipparcos* data (Koen & Eyer 2002).
2. *HD 94910 = AG Car*. This is a W-R thought to be a "hot, quiescent state LBV" (Clark et al. 2010).
3. *HD 50896 = EZ CMa = W-R 6*. Listed as both a W-R and periodic variable super giant, this is a prototype W-R and has a known periodic variability possibly due to a binary companion (Flores et al. 2007).
4. *HD 37151*. Slowly pulsating B stars (SPBs) occur in the same instability strip of the H-R diagram as chemically peculiar B stars (with variability associated with rotation and magnetic fields). The classification of this star is particularly ambiguous (see Briquet et al. 2007 and references therein).
5. *HD 35715*. Is a cataloged Beta Cepheid but is also an ellipsoidal variable (Stankov & Handler 2005). Pulsation was not detected photometrically but in line profiles.
6. *HIP34042 (Z CMa A)*. Is a binary system consisting of a Herbig component (A) and an FU Orionis star (B) in a close orbit. Determining the photometric contributions of the two components separately is problematic because of strong variability and the small angular separation (Millan-Gabet & Monnier 2002).
7. *TV Lyn, UY Cam, V1719 Cyg (HD 200925), and V753 Cen*. Ambiguous classification (within the literature) of RR Lyrae or Delta Scuti-type stars.
8. *IK Hya*. Is a short-period Pop. II Cepheid, making it likely a BL Herculis-type star.

We trained an RF classifier on the features of only the single-labeled stars and then predicted the class probabilities of each label for the doubly labeled stars. This experiment shows that for 7 of the 11 sources, our classifier predicts one of the two classes that the star was originally labeled as. Note that recently, several methods have been developed to classify data with multiple labels (multi-label classification; see Tsoumakas & Katakis 2007), but for the purposes of this work we choose to only perform single-label classification, and remove these data from our sample to avoid biases from inaccurate training labels.

REFERENCES

Bailey, S., Aragon, C., Romano, R., Thomas, R. C., Weaver, B. A., & Wong, D. 2007, ApJ, 665, 1246
Ball, N. M., Brunner, R. J., Myers, A. D., & Tcheng, D. 2006, ApJ, 650, 497
Barning, F. J. M. 1963, Bull. Astron. Inst. Netherlands, 17, 22
Belokurov, V., Evans, N. W., & Du, Y. L. 2003, MNRAS, 341, 1373
Belokurov, V., Evans, N. W., & Le Du, Y. 2004, MNRAS, 352, 233
Blockeel, H., Schietgat, L., Struyf, J., Džeroski, S., & Clare, A. 2006, Knowledge Discovery in Databases: PKDD 2006 (Berlin: Springer-Verlag)
Blomme, J., et al. 2010, ApJ, 713, L204
Breiman, L. 1996, Mach. Learn., 24, 123
Breiman, L. 2001, Mach. Learn., 45, 5
Breiman, L., Friedman, J., Olshen, R., & Stone, C. 1984, Classification and Regression Trees (Boca Raton, FL: Chapman & Hall/CRC)
Brett, D. R., West, R. G., & Wheatley, P. J. 2004, MNRAS, 353, 369
Briquet, M., Hubrig, S., De Cat, P., Aerts, C., North, P., & Schöller, M. 2007, A&A, 466, 269
Burman, P. 1989, Biometrika, 76, 503
Butler, N. R., & Bloom, J. S. 2011, AJ, 141, 93
Cesa-Bianchi, N., Gentile, C., & Zaniboni, L. 2006, J. Mach. Learn. Res., 7, 31
Cheeseman, P., & Stutz, J. 1996, Advances in Knowledge Discovery and Data Mining (Menlo Park, CA: American Association for Artificial Intelligence)
Clark, J. S., Ritchie, B. W., & Negueruela, I. 2010, A&A, 514, A87
Covey, K. R., et al. 2007, AJ, 134, 2398
Debosscher, J., Sarro, L. M., Aerts, C., Cuypers, J., Vandenbussche, B., Garrido, R., & Solano, E. 2007, A&A, 475, 1159
Derekas, A., et al. 2009, MNRAS, 394, 995
Doering, R. L., Meixner, M., Holfeltz, S. T., Krist, J. E., Ardila, D. R., Kamp, I., Clampin, M. C., & Lubow, S. H. 2007, AJ, 133, 2122
Eads, D. R., Williams, S. J., Theiler, J., Porter, R., Harvey, N. R., Perkins, S. J., Brumby, S. P., & David, N. A. 2004, Proc. SPIE, 200, 79
Eyer, L. 2005, in ESA-SP 576, The Three-Dimensional Universe with Gaia, ed. C. Turon, K. S. O'Flaherty, & M. A. C. Perryman (Noordwijk: ESA), 513
Eyer, L. 2006, in ASP Conf. Ser. 349, Astrophysics of Variable Stars, ed. C. Aerts & C. Sterken (San Francisco, CA: ASP), 15
Eyer, L., & Blake, C. 2005, MNRAS, 358, 30
Eyer, L., & Mowlavi, N. 2008, J. Phys. Conf. Ser., 118, 012010
Eyer, L., et al. 2008, in AIP Conf. Proc. 1082, Classification and Discovery in Large Astronomical Surveys, ed. C. A. L. Bailer-Jones (Melville, NY: AIP), 257
Flores, A., Koenigsberger, G., Cardona, O., & de la Cruz, L. 2007, AJ, 133, 2859
Freund, Y., & Schapire, R. 1996, in Machine Learning: Proc. Thirteenth Int. Conf. on Machine Learning, 148
Friedman, J. 1996, Technical Report, Department of Statistics, Stanford Univ.
Friedman, J. H. 2001, Ann. Stat., 29, 1189
Gregory, P. C. 2005, Bayesian Logical Data Analysis for the Physical Sciences: A Comparative Approach with "Mathematica" Support (Cambridge: Cambridge Univ. Press)
Grinin, V. P., Rostopchina, A. N., Barsunova, O. Y., & Demidova, T. V. 2010, Astrophysics, 53, 367
Hastie, T., & Tibshirani, R. 1998, Ann. Stat., 26, 451
Hastie, T., Tibshirani, R., & Friedman, J. 2009, The Elements of Statistical Learning: Data Mining, Inference, and Prediction (2nd ed.; New York: Springer)
Horne, J. H., & Baliunas, S. L. 1986, ApJ, 302, 757
Ivezić, Ž., et al. 2007, AJ, 134, 973

Kessler, R., et al. 2010, PASP, 122, 1415

Knerr, S., et al. 1990, Optim. Meth. Softw., 1, 23

Koen, C., & Eyer, L. 2002, MNRAS, 331, 45

Lomb, N. R. 1976, Ap&SS, 39, 447

LSST Science Collaborations, et al. 2009, arXiv:0912.0201

Mahabal, A., et al. 2008, Astron. Nachr., 329, 288

Marchenko, S. V., Antokhin, I. I., Bertrand, J., Lamontagne, R., Moffat, A. F. J., Piceno, A., & Matthews, J. M. 1994, AJ, 108, 678

Millan-Gabet, R., & Monnier, J. D. 2002, ApJ, 580, L167

Moffat, A. F. J., et al. 2008, ApJ, 679, L45

O'Keefe, P. J., Gowanlock, M. G., McConnell, S. M., & Patton, D. 2009, in ASP Conf. Ser. 411, Astronomical Data Analysis Software and Systems XVIII, ed. D. A. Bohlender, D. Durand, & P. Dowler (San Francisco, CA: ASP), 318

Paunzen, E., & Reegen, P. 2008, Commun. Asteroseismol., 153, 49

Perryman, M., et al. 1997, A&A, 323, L49

Press, W., Vetterling, W., Teukolsky, S., & Flannery, B. 2001, Numerical Recipes in C++: The Art of Scientific Computing (New York: Cambridge Univ. Press)

Protopapas, P., Giammarco, J. M., Faccioli, L., Struble, M. F., Dave, R., & Alcock, C. 2006, MNRAS, 369, 677

Quinlan, J. 1996, in Proc. Thirteenth National Conf. on Artificial Intelligence (American Association for Artificial Intelligence), 725

Rebbapragada, U., Protopapas, P., Brodley, C. E., & Alcock, C. 2009, in ASP Conf. Ser. 411, Astronomical Data Analysis Software and Systems XVIII, ed. D. A. Bohlender, D. Durand, & P. Dowler (San Francisco, CA: ASP), 264

Rodríguez, E., López-González, M. J., & López de Coca, P. 2000, A&AS, 144, 469

Sarro, L. M., Debosscher, J., López, M., & Aerts, C. 2009, A&A, 494, 739

Scargle, J. D. 1982, ApJ, 263, 835

Sesar, B., et al. 2007, AJ, 134, 2236

Shin, M., Sekora, M., & Byun, Y. 2009, MNRAS, 400, 1897

Silla, C., & Freitas, A. 2011, Data Mining Knowl. Discovery, 22, 31

Stankov, A., & Handler, G. 2005, ApJS, 158, 193

Stetson, P. B. 1996, PASP, 108, 851

Suchkov, A. A., Hanisch, R. J., & Margon, B. 2005, AJ, 130, 2439

Tsoumakas, G., & Katakis, I. 2007, Int. J. Data Warehousing Mining, 3, 1

Udalski, A., Soszynski, I., Szymanski, M., Kubiak, M., Pietrzynski, G., Wozniak, P., & Zebrun, K. 1999,

Vapnik, V. 2000, The Nature of Statistical Learning Theory (New York: Springer)

Vens, C., Struyf, J., Schietgat, L., Džeroski, S., & Blockeel, H. 2008, Mach. Learn., 73, 185

Walkowicz, L. M., et al. 2009, arXiv:0902.3981

Wasserman, L. 2006, All of Nonparametric Statistics (New York: Springer)

Whitelock, P. A., Feast, M. W., & van Leeuwen, F. 2008, MNRAS, 386, 313

Willemsen, P. G., & Eyer, L. 2007, arXiv:0712.2898

Woźniak, P. R., Williams, S. J., Vestrand, W. T., & Gupta, V. 2004, AJ, 128, 2965

Wu, T., Lin, C., & Weng, R. 2004, J. Mach. Learn. Res., 5, 975

Yankov, D., Keogh, E., & Rebbapragada, U. 2008, Knowl. Inf. Syst., 17, 241

Zechmeister, M., & Kürster, M. 2009, A&A, 496, 577